7. Talati G, Ohta A, Rai T, Sohara E, Naito S, Vandewalle A, Sasaki S, Uchida S. Effect of angiotensin II on the WNK-OSR1/SPAK-NCC phosphorylation cascade in cultured mpkDCT cells and in vivo mouse kidney. *Biochem Biophys Res Commun*. 2010;393:844–848.
8. San-Cristobal P, Pacheco-Alvarez D, Richardson C, Ring AM, Vazquez N, Rafiqi FH, Chari D, Kahle KT, Leng Q, Bobadilla NA, Hebert SC, Alessi DR, Lifton RP, Gamba G. Angiotensin II signaling increases activity of the renal Na-Cl cotransporter through a WNK4-SPAK-dependent pathway. *Proc Natl Acad Sci U S A*. 2009;106:4384–4389.
9. Sandberg MB, Riquier AD, Pihakaski-Maunsbach K, McDonough AA, Maunsbach AB. ANG II provokes acute trafficking of distal tubule Na+-Cl(-) cotransporter to apical membrane. *Am J Physiol Renal Physiol*. 2007;293:F662--F669.
10. Naito S, Ohta A, Sohara E, Ohta E, Rai T, Sasaki S, Uchida S. Regulation of WNK1 kinase by extracellular potassium. *Clin Exp Nephrol*. 2011;15:195–202.
11. Vallon V, Schroth J, Lang F, Kuhl D, Uchida S. Expression and phosphorylation of the Na+-Cl- cotransporter NCC in vivo is regulated by dietary salt, potassium, and SGK1. *Am J Physiol Renal Physiol*. 2009;297:F704--F712.
12. Eckel RH, Grundy SM, Zimmet PZ. The metabolic syndrome. *Lancet*. 2005;365:1415–1428.
13. Chen J, Gu D, Huang J, Rao DC, Jaquish CE, Hixson JE, Chen CS, Lu F, Hu D, Rice T, Kelly TN, Hamm LL, Whelton PK, He J, for the GenSalt Collaborative Research Group. Metabolic syndrome and salt sensitivity of blood pressure in non-diabetic people in China: a dietary intervention study. *Lancet*. 2009;373:829–835.
14. Galletti F, Strazzullo P, Ferrara I, Annuzzi G, Rivellese AA, Gatto S, Mancini M. NaCl sensitivity of essential hypertensive patients is related to insulin resistance. *J Hypertens*. 1997;15:1485–1491.
15. Shimamoto K, Hirata A, Fukuoka M, Higashiura K, Miyazaki Y, Shiiki M, Masuda A, Nakagawa M, Iimura O. Insulin sensitivity and the effects of insulin on renal sodium handling and pressor systems in essential hypertensive patients. *Hypertension*. 1994;23:I29–33.
16. DeFronzo RA, Cooke CR, Andres R, Faloona GR, Davis PJ. The effect of insulin on renal handling of sodium, potassium, calcium, and phosphate in man. *J Clin Invest*. 1975;55:845–855.
17. DeFronzo RA, Goldberg M, Agus ZS. The effects of glucose and insulin on renal electrolyte transport. *J Clin Invest*. 1976;58:83–90.
18. Tiwari S, Nordquist L, Halagappa VK, Ecelbarger CA. Trafficking of ENaC subunits in response to acute insulin in mouse kidney. *Am J Physiol Renal Physiol*. 2007;293:F178--F185.
19. Song J, Hu X, Riazi S, Tiwari S, Wade JB, Ecelbarger CA. Regulation of blood pressure, the epithelial sodium channel (ENaC), and other key renal sodium transporters by chronic insulin infusion in rats. *Am J Physiol Renal Physiol*. 2006;290:F1055--F1064.
20. Sohara E, Rai T, Yang SS, Ohta A, Naito S, Chiga M, Nomura N, Lin SH, Vandewalle A, Ohta E, Sasaki S, Uchida S. Acute insulin stimulation induces phosphorylation of the Na-Cl cotransporter in cultured distal mpkDCT cells and mouse kidney. *PLoS One*. 2011;6:e24277.
21. Chen H, Charlat O, Tartaglia LA, Woolf EA, Weng X, Ellis SJ, Lakey ND, Culpepper J, Moore KJ, Breitbart RE, Duyk GM, Tepper RI, Morgenstern JP. Evidence that the diabetes gene encodes the leptin receptor: identification of a mutation in the leptin receptor gene in db/db mice. *Cell*. 1996;84:491–495.
22. Shibuya K, Kanasaki K, Isono M, Omata M, Sugimoto T, Araki S, Isshiki K, Kashiwagi A, Haneda M, Koya D. *N*-Acetyl-seryl-aspartyl-lysyl-proline prevents renal insufficiency and mesangial matrix expansion in diabetic db/db mice. *Diabetes*. 2005;54:838–845.
23. Chin M, Isono M, Isshiki K, Araki S, Sugimoto T, Guo B, Sato H, Haneda M, Kashiwagi A, Koya D. Estrogen and raloxifene, a selective estrogen receptor modulator, ameliorate renal damage in db/db mice. *Am J Pathol*. 2005;166:1629–1636.
24. Hirata K, Kume S, Araki S, Sakaguchi M, Chin-Kanasaki M, Isshiki K, Sugimoto T, Nishiyama A, Koya D, Haneda M, Kashiwagi A, Uzu T. Exendin-4 has an anti-hypertensive effect in salt-sensitive mice model. *Biochem Biophys Res Commun*. 2009;380:44–49.
25. Rutkai I, Feher A, Erdei N, Henrion D, Papp Z, Edes I, Koller A, Kaley G, Bagi Z. Activation of prostaglandin E2 EP1 receptor increases arteriolar tone and blood pressure in mice with type 2 diabetes. *Cardiovasc Res*. 2009;83:148–154.
26. Senador D, Kanakamedala K, Irigoyen MC, Morris M, Elased KM. Cardiovascular and autonomic phenotype of db/db diabetic mice. *Exp Physiol*. 2009;94:648–658.
27. Rafiqi FH, Zuber AM, Glover M, Richardson C, Fleming S, Jovanovic S, Jovanovic A, O'Shaughnessy KM, Alessi DR. Role of the WNK-activated SPAK kinase in regulating blood pressure. *EMBO Mol Med*. 2010;2:63–75.
28. Alessi DR, Andjelkovic M, Caudwell B, Cron P, Morrice N, Cohen P, Hemmings BA. Mechanism of activation of protein kinase B by insulin and IGF-1. *EMBO J*. 1996;15:6541–6551.
29. Alessi DR, Downes CP. The role of PI 3-kinase in insulin action. *Biochim Biophys Acta*. 1998;1436:151–164.
30. Lawlor MA, Alessi DR. PKB/Akt: a key mediator of cell proliferation, survival and insulin responses? *J Cell Sci*. 2001;114:2903–2910.
31. Zdychová J, Komers R. Emerging role of Akt kinase/protein kinase B signaling in pathophysiology of diabetes and its complications. *Physiol Res*. 2005;54:1–16.
32. Maira SM, Stauffer F, Brueggen J, Furet P, Schnell C, Fritsch C, Brachmann S, Chene P, De Pover A, Schoemaker K, Fabbro D, Gabriel D, Simonen M, Murphy L, Finan P, Sellers W, Garcia-Echeverria C. Identification and characterization of NVP-BEZ235, a new orally available dual phosphatidylinositol 3-kinase/mammalian target of rapamycin inhibitor with potent in vivo antitumor activity. *Mol Cancer Ther*. 2008;7:1851–1863.
33. Cho DC, Cohen MB, Panka DJ, Collins M, Ghebremichael M, Atkins MB, Signoretti S, Mier JW. The efficacy of the novel dual PI3-kinase/mTOR inhibitor NVP-BEZ235 compared with rapamycin in renal cell carcinoma. *Clin Cancer Res*. 2010;16:3628–3638.
34. Faber AC, Li D, Song Y, Liang MC, Yeap BY, Bronson RT, Lifshits E, Chen Z, Maria SM, Garcia-Echeverria C, Wong KK, Engelman JA. Differential induction of apoptosis in HER2 and EGFR addicted cancers following PI3K inhibition. *Proc Natl Acad Sci U S A*. 2009;106:19503–19508.
35. Garcia-Martinez JM, Wullschleger S, Preston G, Guichard S, Fleming S, Alessi DR, Duce SL. Effect of PI3K- and mTOR-specific inhibitors on spontaneous B-cell follicular lymphomas in PTEN/LKB1-deficient mice. *Br J Cancer*. 2011;104:1116–1125.
36. Raynaud FI, Eccles SA, Patel S, Alix S, Box G, Chuckowree I, Folkes A, Gowan S, Ds Haven Brandon A, Di Stefano F, Hayes A, Henley AT, Lensun L, Pergl-Wilson G, Robson A, Saghir N, Zhyvoloup A, McDonald E, Sheldrake P, Shuttleworth S, Valenti M, Wan NC, Clarke PA, Workman P. Biological properties of potent inhibitors of class I phosphatidylinositide 3-kinases: from PI-103 through PI-540, PI-620 to the oral agent GDC-0941. *Mol Cancer Ther*. 2009;8:1725–1738.
37. Meng J, Dai B, Fang B, Bekele BN, Bornmann WG, Sun D, Peng Z, Herbst RS, Papadimitrakopoulou V, Minna JD, Peyton M, Roth JA. Combination treatment with MEK and AKT inhibitors is more effective than each drug alone in human non-small cell lung cancer in vitro and in vivo. *PLoS One*. 2010;5:e14124.
38. Hirai H, Sootome H, Nakatsuru Y, Miyama K, Taguchi S, Tsujioka K, Ueno Y, Hatch H, Majumder PK, Pan BS, Kotani H. MK-2206, an allosteric Akt inhibitor, enhances antitumor efficacy by standard chemotherapeutic agents or molecular targeted drugs in vitro and in vivo. *Mol Cancer Ther*. 2010;9:1956–1967.
39. Smith GC, Ong WK, Rewcastle GW, Kendall JD, Han W, Shepherd PR. Effects of acutely inhibiting PI3K isoforms and mTOR on regulation of glucose metabolism in vivo. *Biochem J*. 2012;442:161–169.
40. Lakka HM, Laaksonen DE, Lakka TA, Niskanen LK, Kumpusalo E, Tuomilehto J, Salonen JT. The metabolic syndrome and total and cardiovascular disease mortality in middle-aged men. *JAMA*. 2002;288:2709–2716.
41. Weinberger MH, Fineberg NS, Fineberg SE, Weinberger M. Salt sensitivity, pulse pressure, and death in normal and hypertensive humans. *Hypertension*. 2001;37:429–432.
42. Kuroda S, Uzu T, Fujii T, Nishimura M, Nakamura S, Inenaga T, Kimura G. Role of insulin resistance in the genesis of sodium sensitivity in essential hypertension. *J Hum Hypertens*. 1999;13:257–262.
43. Feliers D, Duraisamy S, Faulkner JL, Duch J, Lee AV, Abboud HE, Choudhury GG, Kasinath BS. Activation of renal signaling pathways in db/db mice with type 2 diabetes. *Kidney Int*. 2001;60:495–504.
44. Catena C, Cavarape A, Novello M, Giacchetti G, Sechi LA. Insulin receptors and renal sodium handling in hypertensive fructose-fed rats. *Kidney Int*. 2003;64:2163–2171.
45. Sechi LA, Griffin CA, Giacchetti G, Zingaro L, Catena C, Bartoli E, Schambelan M. Abnormalities of insulin receptors in spontaneously hypertensive rats. *Hypertension*. 1996;27:955–961.

46. Shao J, Yamashita H, Qiao L, Friedman JE. Decreased Akt kinase activity and insulin resistance in C57BL/KsJ-Leprdb/db mice. *J Endocrinol.* 2000;167:107–115.
47. Chakraborty A, Koldobskiy MA, Bello NT, Maxwell M, Potter JJ, Juluri KR, Maag D, Kim S, Huang AS, Dailey MJ, Saleh M, Snowman AM, Moran TH, Mezey E, Snyder SH. Inositol pyrophosphates inhibit Akt signaling, thereby regulating insulin sensitivity and weight gain. *Cell.* 2010;143:897–910.
48. Wang RH, Kim HS, Xiao C, Xu X, Gavrilova O, Deng CX. Hepatic Sirt1 deficiency in mice impairs mTorc2/Akt signaling and results in hyperglycemia, oxidative damage, and insulin resistance. *J Clin Invest.* 2011;121:4477–4490.
49. Schnyder B, Pittet M, Durand J, Schnyder-Candrian S. Rapid effects of glucose on the insulin signaling of endothelial NO generation and epithelial Na transport. *Am J Physiol Endocrinol Metab.* 2002;282:E87--E94.
50. Rozansky DJ, Cornwall T, Subramanya AR, Rogers S, Yang YF, David LL, Zhu X, Yang CL, Ellison DH. Aldosterone mediates activation of the thiazide-sensitive Na-Cl cotransporter through an SGK1 and WNK4 signaling pathway. *J Clin Invest.* 2009;119:2601–2612.
51. Ring AM, Leng Q, Rinehart J, Wilson FH, Kahle KT, Hebert SC, Lifton RP. An SGK1 site in WNK4 regulates Na+ channel and K+ channel activity and has implications for aldosterone signaling and K+ homeostasis. *Proc Natl Acad Sci U S A.* 2007;104:4025–4029.
52. Vitari AC, Deak M, Collins BJ, Morrice N, Prescott AR, Phelan A, Humphreys S, Alessi DR. WNK1, the kinase mutated in an inherited high-blood-pressure syndrome, is a novel PKB (protein kinase B)/Akt substrate. *Biochem J.* 2004;378:257–268.
53. Komers R, Rogers S, Oyama TT, Xu B, Yang CL, McCormick J, Ellison DH. Enhanced phosphorylation of Na-Cl cotransporter in experimental metabolic syndrome: role of insulin. *Clin Sci (Lond).* 2012; 123:635–647.

Novelty and Significance

What Is New?

- It was determined that increased NCC phosphorylation in db/db mice is regulated by the PI3K/Akt signaling pathway. Moreover, the PI3K-Akt-WNK-OSR1/SPAK-NCC signaling cascade plays an essential physiological role in salt-sensitive hypertension under hypersinsulinemic conditions.

What Is Relevant?

- It has been reported that the metabolic syndrome enhances salt sensitivity, leading to salt-sensitive hypertension. The metabolic syndrome causes hyperinsulinemia as a result of insulin resistance, and hyperinsulinemia causes an aberrant increase in sodium reabsorption by the kidney. We discovered that hyperinsulinemia in db/db mice can activate NCC through the PI3K-Akt-WNK-SPAK/OSR1-NCC signaling cascade. Because the same mechanism has been proven to be the cause of human hypertension (PHAII), this cascade may be one factor operating in the development of salt-sensitive hypertension in human hyperinsulinemic conditions.

Summary

In this article, we report that the PI3K/Akt signaling pathway activates the WNK-OSR1/SPAK-NCC phosphorylation cascade in hyperinsulinemic db/db mice. This mechanism may play a role in the pathogenesis of salt-sensitive hypertension in human hyperinsulinemic conditions, such as the metabolic syndrome.

J Bone Miner Metab (2012) 30:238–242
DOI 10.1007/s00774-011-0320-6

CASE REPORT

Severe hyperparathyroidism in a pre-dialysis chronic kidney disease patient treated with a very low protein diet

Eriko Ohta · Masanobu Akazawa · Yumi Noda · Shintaro Mandai · Shotaro Naito · Akihito Ohta · Eisei Sohara · Tomokazu Okado · Tatemitsu Rai · Shinichi Uchida · Sei Sasaki

Received: 27 January 2011 / Accepted: 28 August 2011 / Published online: 12 October 2011

Abstract The present report describes a case of a 64-year-old pre-dialysis woman with chronic kidney disease (CKD) stage 5, who developed severe hyperparathyroidism. This patient had been on a very low protein diet (VLPD) to delay the progression of CKD and the need for renal replacement therapy (RRT). Her serum calcium levels were high-normal to slightly high during this time. However, her serum intact parathyroid hormone (PTH) levels increased from 400 to 1160 pg/ml rapidly over a period of 3 months. Serum 1,25-(OH)2D levels were low, and ultrasound of the neck showed three markedly enlarged parathyroid glands exceeding 2 cm. Parathyroidectomy was performed, and all glands showed nodular hyperplasia, which indicated severe secondary hyperparathyroidism leading to tertiary. Severe secondary hyperparathyroidism requiring surgical intervention is usually observed in patients with long-term RRT and is relatively rare in the pre-dialysis patient. In this case, extension of the pre-dialysis period by VLPD may have predisposed this patient to develop severe secondary hyperparathyroidism. Thus, careful monitoring of calcium, phosphorus, and PTH may be necessary in patients treated with VLPD even before renal replacement therapy. Furthermore, initiation of dialysis should not be excessively delayed by strict protein restriction dietary therapy.

Keywords Pre-dialysis patient · Secondary hyperparathyroidism · Very low protein diet · Vitamin D insufficiency

E. Ohta (✉) · M. Akazawa · Y. Noda · S. Mandai · S. Naito · A. Ohta · E. Sohara · T. Okado · T. Rai · S. Uchida · S. Sasaki
Department of Nephrology, Tokyo Medical and Dental University, 1-5-45 Yushima, Bunkyo, Tokyo 113-8519, Japan
e-mail: eohta.kid@tmd.ac.jp

Introduction

Secondary hyperparathyroidism is a frequent complication of chronic kidney disease (CKD), and the concordance of these two diseases is known as chronic kidney disease-mineral and bone disorder (CKD-MBD). The pathophysiology of CKD-MBD is related to CKD-induced phosphorus retention, which leads to elevation of fibroblast growth factor-23 levels followed by decreased vitamin D activity and hypocalcemia [1]. This results in stimulation of the parathyroid glands, and hypersecretion of parathyroid hormone (PTH). Severe secondary hyperparathyroidism requiring surgical intervention is seen most frequently in patients undergoing long-term renal replacement therapy (RRT), but is exceedingly rare in pre-dialysis patients [2, 3].

The present report describes a patient with CKD who had been undergoing a very low protein diet (VLPD) to delay the progression of CKD and the need for RRT, and who subsequently developed severe secondary hyperparathyroidism.

Case report

A female patient was noted to have hematoproteinuria in her youth, but did not undergo detailed examinations or any therapies at that time. At the age of 49, her serum creatinine (Cr) level increased to 1.6 mg/dl, and a low protein diet (target protein intake was 40 g/day) was introduced for the treatment of CKD. However, her renal function continued to gradually deteriorate. At the age of 61, her serum Cr was >7 mg/dl, and a VLPD (25 g/day) was instituted in an effort to delay the need for dialysis. A 24-h urine collection indicated good compliance and good response to strict dietary therapy; protein intake estimated from urine excretion of urea nitrogen was 21–24 g/day, salt

intake was 4–5 g/day, potassium (K) intake was only 8–17 mEq/day and phosphorus (iP) intake was only 150–280 mg/day. Her serum Cr levels remained stable in the range of 7–8 mg/dl for 3 years, and her blood urea nitrogen (BUN) decreased significantly (from >80 mg/dl to approximately 50 mg/dl). In response to diet therapy alone, serum iP levels remained within the normal range (3.5–4.6 mg/dl), and serum calcium (Ca) levels were maintained in the high-normal range (10.0–10.4 mg/dl). Therefore, neither vitamin D nor phosphate binders were prescribed during the clinical course. The patient did not experience hypocalcemia at any point.

At the end of 2009, the patient's serum intact PTH levels rapidly increased from 400 to 1160 pg/ml over a period of 3 months without any apparent symptoms. In January 2010, she was referred to our institution and admitted to our hospital. Changes in laboratory values before admission are shown in Fig. 1.

On admission, the patient looked well and appeared alert. She was 159 cm tall and weighed 58 kg. Her blood pressure was 140/86 mmHg, her pulse was regular at 90 beats per minute, and her body temperature was 36.6°C. There was no obvious swelling of the neck or peripheral edema. There was no family history of renal diseases, hypercalcemia or endocrine diseases, and she did not have any other past history except for CKD.

Hematology testing yielded the following results: red blood cell count, 304 × 10^4/μl; hemoglobin, 9.4 g/dl; white blood cell count, 5200/μl; and platelet count, 11.1 × 10^6/μl. Serum biochemical analysis showed the following results: albumin, 3.9 g/dl; BUN, 50 mg/dl; Cr, 7.9 mg/dl; uric acid (UA), 6.6 mg/dl; sodium (Na), 140 mEq/l; K, 4.5 mEq/l; chloride (Cl), 106 mEq/l; Ca, 10.8 mg/dl; iP, 4.5 mg/dl; magnesium (Mg), 3.3 mg/dl, alkaline phosphatase (ALP), 352 U/l; and C-reactive protein (CRP), 0.03 mg/dl. Endocrine tests showed that intact PTH was 1160 pg/ml; 1,25-(OH)2D was < 10 pg/ml (standard range 20–60 pg/ml); and PTH-related protein was <1.1 pmol/l. Other hormones, such as anterior pituitary hormones and thyroid hormones, were within normal limits. Urine tests showed proteinuria of 0.3 g/day, and creatinine clearance was decreased at 5 ml/min.

Ultrasound of the neck revealed that the right lower and left upper glands were markedly enlarged at

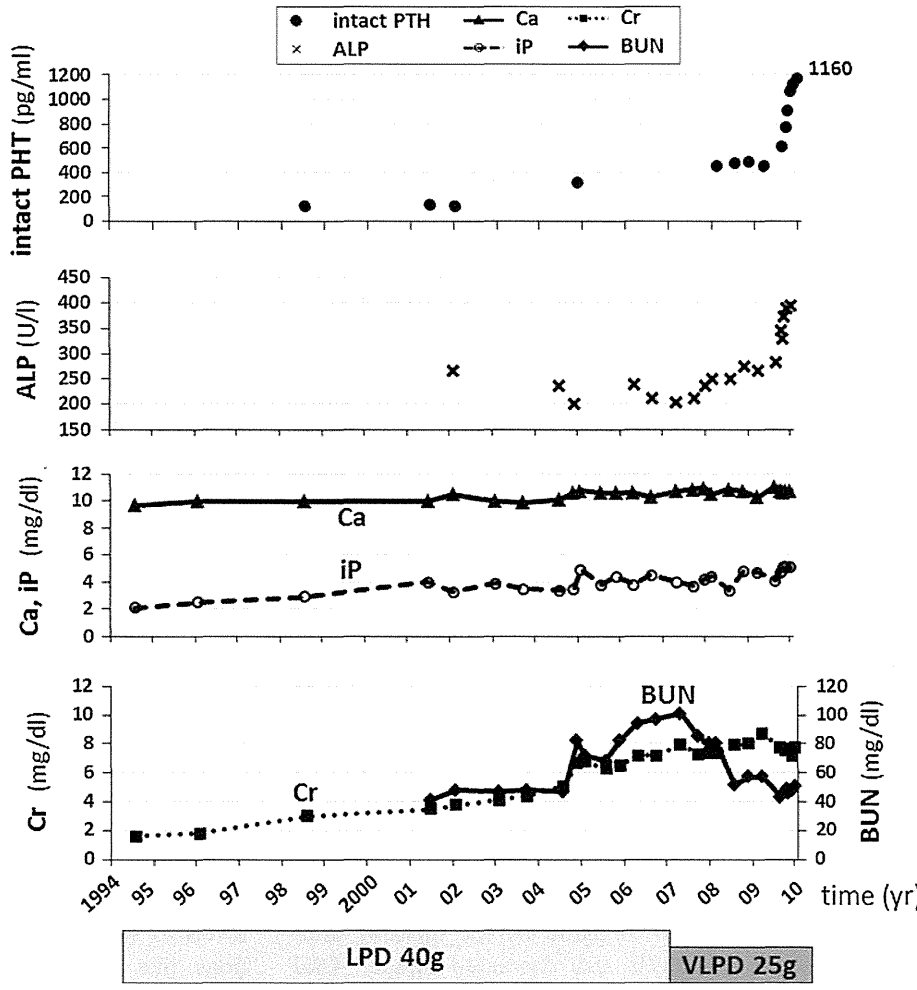

Fig. 1 Time course of serum intact PTH, ALP, Ca, iP, BUN and Cr levels before admission. *LPD* low protein diet, *VLPD* very low protein diet

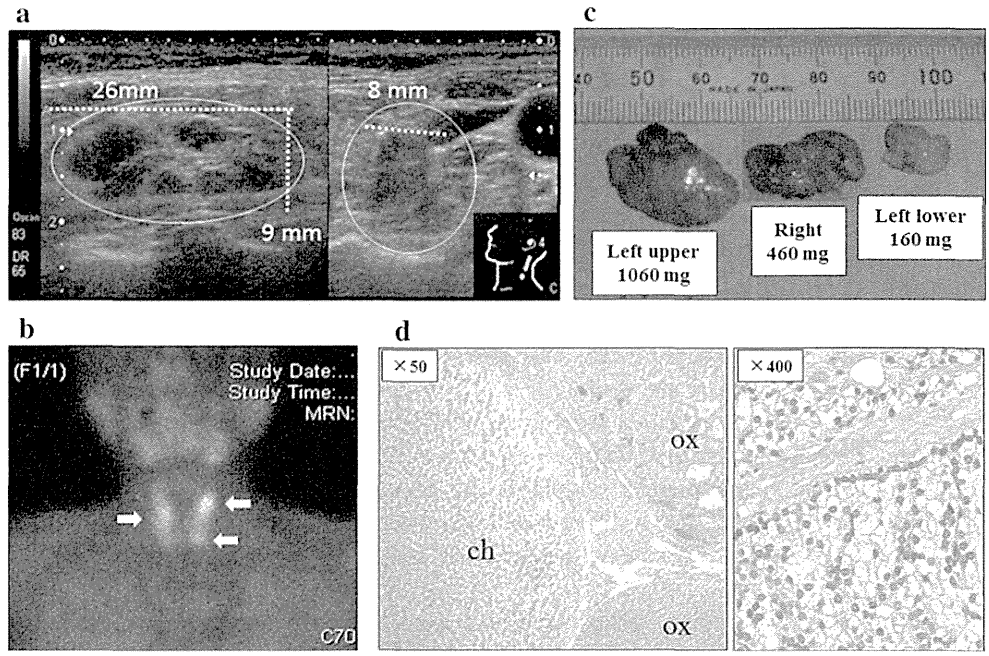

Fig. 2 **a** Ultrasound of the left upper parathyroid grand. **b** Scintigraphy with technetium-99 m labeled methoxy-isobutyl-isonitrile. **c** Gross specimen of the parathyroid glands after surgery. **d** Light microscopic examination showed nodular hyperplasia with chief cells and oxyphil cells in all glands (H&E staining, original magnification ×50 and ×400). *ch* nodule mainly formed with chief cells, *ox* nodule mainly formed with oxyphil cells

23 × 8 × 6 mm and 26 × 9 × 8 mm in size, respectively (Fig. 2a). Scintigraphy with technetium-99 m labeled methoxy-isobutyl-isonitrile demonstrated intense uptake in both right lower and left upper glands but did not show any abnormal uptake in other organs (Fig. 2b). Chest X-ray, electrocardiogram and echocardiogram showed no abnormality. Bone mineral density of the left femoral neck measured by dual-energy X-ray absorptiometry was 0.58 g/cm^2, which was only 64% of the predicted young adult mean and which was consistent with pathological bone loss. Computed tomography of the whole body did not show any other tumors or abnormalities, except for partial moderate aortic calcification. Multiple endocrine neoplasia (MEN) was excluded by clinical imaging and hematological examination. The absence of a family history of hypercalcemia or endocrine diseases also supported the absence of MEN. Because of the size of parathyroid glands and the elevation in serum Ca and iP, parathyroidectomy (PTx) was performed in February 2010.

The resected parathyroid glands are shown in Fig. 2c. Three glands (one right gland and two left glands) were localized, and all were enlarged. The largest was the left upper gland (1060 mg), followed by the right gland (460 mg) and the left lower gland (160 mg). A small part of the left lower gland was reimplanted into the forearm muscle. Light microscopic examination (Fig. 2d) revealed nodular hyperplasia with chief cells and oxyphil cells in all glands. No findings of adenoma, dysplasia, malignancy or atrophy were present.

Laboratory data after PTx are presented in Fig. 3. Serum intact PTH decreased to 92 pg/ml by the morning after PTx, and serum Ca levels also decreased rapidly. Oral vitamin D and calcium lactate was initiated to prevent hungry bone syndrome and to maintain appropriate values of serum Ca, iP and intact PTH. Ca was maintained at <10 mg/dl, and iP was maintained at <4 mg/dl. The patient was discharged 14 days after surgery.

Subsequent follow-up revealed that serum ALP levels gradually decreased to 200–250 U/l. The patient did well as an outpatient, but renal function continued to deteriorate. Her Cr levels progressively increased on every follow-up, and she was excessively preoccupied regarding potential exacerbation of secondary hyperparathyroidism. Four months after PTx, when Cr was >10 mg/dl, the patient experienced loss of appetite, and her serum intact PTH levels were 100–200 pg/ml, which was somewhat high for patients after PTx. Further delay in initiation of dialysis was not thought to be beneficial for this patient, and thus, hemodialysis therapy was initiated.

Discussion

Secondary hyperparathyroidism is a known complication of CKD. Increasing levels of intact PTH have also been reported to be associated with a significantly elevated risk of mortality and need for RRT [4]. Severe secondary hyperparathyroidism necessitating PTx rarely occurs in the pre-dialysis period [2, 3]. Furthermore, secondary hyperparathyroidism without hypocalcemia or hyperphosphatemia is even rarer in pre-dialysis patients, which means that parathyroid tissue, with failure of increasing serum calcium levels to suppress secretion of PTH, autonomously functions like primary or tertiary hyperparathyroidism. In

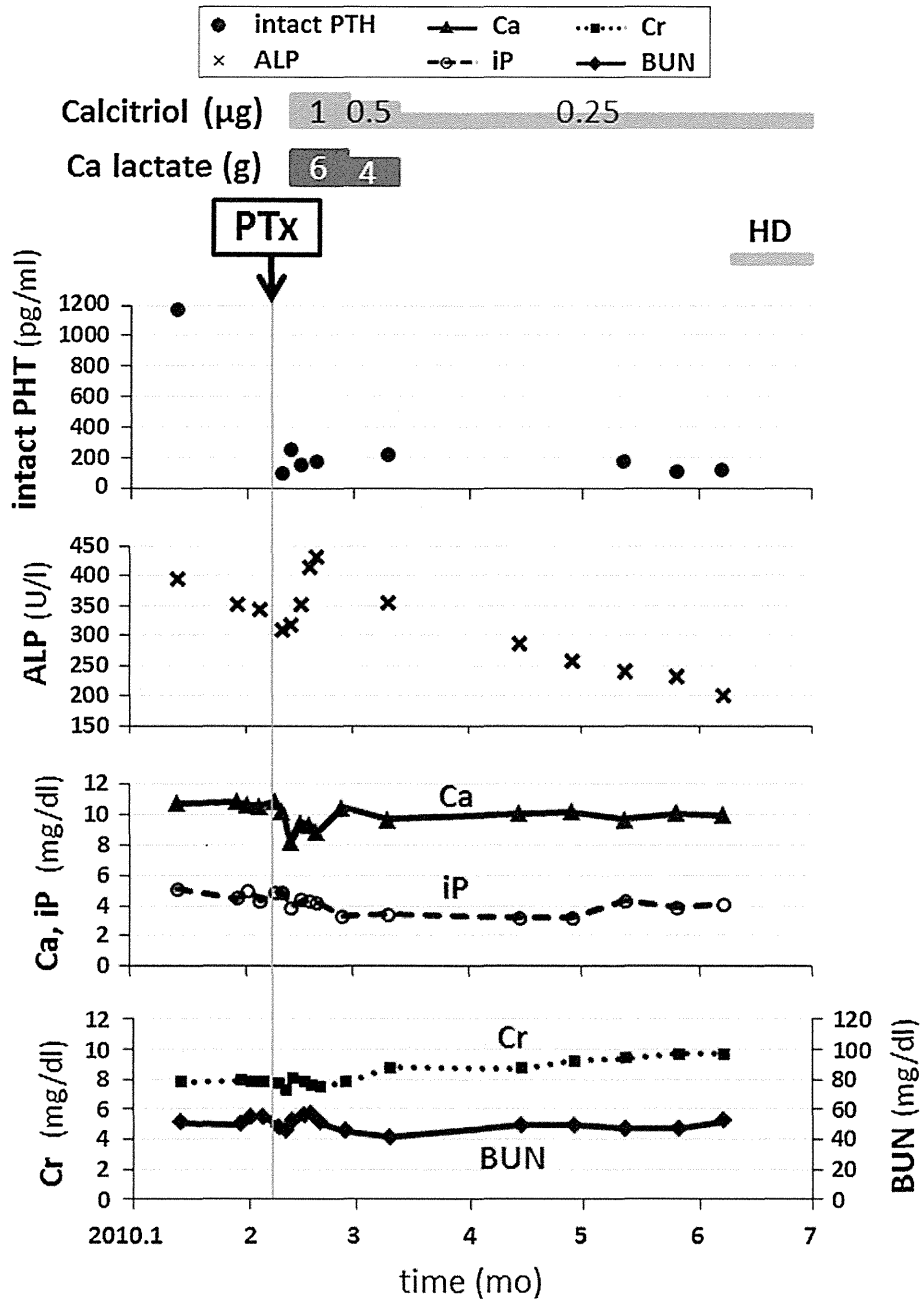

Fig. 3 Serum intact PTH, ALP, Ca, iP, BUN and Cr levels after parathyroidectomy (PTx)

particular, the phenomenon in the present case in which serum intact PTH levels rapidly increased at the end of 2009 might indicate that the parathyroid tissue had acquired autonomous function.

To our knowledge, only one similar case has been reported in which a patient also developed severe secondary hyperparathyroidism with mild hypercalcemia (Ca 10.9 mg/dl) in the pre-dialysis stage [2]. In contrast to the present case, that patient showed severe hyperphosphatemia (iP 9.9 mg/dl), bone pain, and radiographic evidence of bony destruction. Furthermore, the patient was already in end-stage renal failure at initial presentation, with severe anemia (Hb 4.5 g/dl), and was immediately started on hemodialysis. PTx was performed after the initiation of dialysis therapy. The authors suggested that the patient had a long history of CKD with severe untreated hyperphosphatemia and likely had hypocalcemia in the past, all of which led to severe secondary hyperparathyroidism. Histological findings included hyperplasia of all glands as well as an adenoma-like portion, which the author speculated could be an incidental solitary PTH-producing adenoma.

In the present case, our patient had engaged in a VLPD for several years, there was no history of hypocalcemia or hyperphosphatemia, and serum vitamin D level was low;

thus, our patient may have developed severe secondary hyperparathyroidism secondary to vitamin D insufficiency resulting from prolonged and advanced uremic conditions. Previous studies have reported that low vitamin D status directly affects and stimulates parathyroid glands [5]. This supposition is also consistent with histopathological findings of parathyroid hyperplasia without any findings of adenoma. In a recent animal study, dietary protein and dietary phosphorus played an important role in the progression of CKD and secondary hyperparathyroidism [6]. In this case, secondary hyperparathyroidism progressed despite restriction of dietary protein and phosphorus, suggesting that vitamin D insufficiency was present.

The possibility of primary hyperparathyroidism can still not be definitively excluded, as there are several reports that low vitamin D status also causes and aggravates primary hyperparathyroidism [7, 8]. However, if primary hyperparathyroidism was present in this case, then higher serum Ca levels would be expected. Moreover, the most common histology associated with primary hyperparathyroidism is single gland adenoma (75–85%), followed by multi-gland adenoma (two glands in 2–12% of cases, three glands in <1–2%, and four or more in <1%), and carcinoma (<1%). In contrast, hyperplasia is relatively uncommon (<10%) [9, 10]. Mizumoto et al. [3] described five cases of primary hyperparathyroidism accompanied by CKD; adenoma was present in the biggest gland in all four of the patients that underwent PTx. Moreover, elevation of Ca and iP in combination with high ALP indicates bone reabsorption in response to high PTH and osteitis fibrosa. This phenomenon is common in patients with severe secondary hyperparathyroidism. Taken in combination, these observations suggest that a diagnosis of secondary hyperparathyroidism is most likely in the present case. Even if primary hyperparathyroidism was also present incidentally, the main pathology of the present case was certainly secondary hyperparathyroidism caused by CKD.

The optimal time to initiate RRT remains controversial. For example, some studies suggest that early initiation of dialysis for end-stage kidney disease results in improved morbidity, mortality and quality of life [11, 12], while others do not [13, 14], or suggest that early initiation of hemodialysis can be harmful [15]. Regardless, the present case illustrates that excessive prolongation of the pre-dialysis period and advanced uremic condition using dietary restrictions can lead to severe secondary hyperparathyroidism despite adequate control of serum Ca and iP levels.

In summary, we described a case of severe secondary hyperparathyroidism that occurred in a pre-dialysis patient in the absence of hypocalcemia and hyperphosphatemia. In this case, strict dietary restriction led to prolonged uremic conditions and ultimately to secondary hyperparathyroidism requiring PTx even in the pre-dialysis period. Thus, initiation of dialysis should not be excessively delayed by strict protein restriction dietary therapy.

References

1. Martin KJ, Gonzalez EA (2011) Prevention and control of phosphate retention/hyperphosphatemia in CKD-MBD: what is normal, when to start, and how to treat? Clin J Am Soc Nephrol 6:440–446
2. Takasaki I, Shionoiri H, Yabana M, Takagi N, Kamijo S, Nakatani Y, Umemura S (1999) Severe hyperparathyroidism with hypercalcemia associated with chronic renal failure at pre-dialysis stage. Endocrinol J 46:167–171
3. Mizumoto D, Watanabe Y, Fukuzawa Y, Aoi N, Yamazaki C (1994) Clinical profile and outcome of primary hyperparathyroidism accompanied by chronic renal failure. Clin Nephrol 42:315–321
4. Smith DH, Johnson ES, Thorp ML, Yang X, Neil N (2009) Hyperparathyroidism in chronic kidney disease: a retrospective cohort study of costs and outcomes. J Bone Miner Metab 27:287–294
5. Breslau NA (1988) Normal and abnormal regulation of 1,25-(OH)2D synthesis. Am J Med Sci 296:417–425
6. Kusano K, Segawa H, Ohnishi R, Fukushima N, Miyamoto K (2008) Role of low protein and low phosphorus diet in the progression of chronic kidney disease in uremic rats. J Nutr Sci Vitaminol 54:237–243
7. Silverberg SJ, Vitamin D (2007) Deficiency and primary hyperparathyroidism. J Bone Miner Res 2(22 Suppl):V100–V104
8. Silverberg SJ, Shane E, Dempster DW, Bilezikian JP (1999) The effects of vitamin D insufficiency in patients with primary hyperparathyroidism. Am J Med 107:561–567
9. Fraser WD (2009) Hyperparathyroidism. Lancet 374:145–158
10. Carlson D (2010) Parathyroid pathology: hyperparathyroidism and parathyroid tumors. Arch Pathol Lab Med 134:1639–1644
11. Hakim RM, Lazarus JM (1995) Initiation of dialysis. J Am Soc Nephrol 6:1319–1328
12. Churchill DN (1997) An evidence-based approach to earlier initiation of dialysis. Am J Kidney Dis 30:899–906
13. Cooper BA, Branley P, Bulfone L, Collins JF, Craig JC, Fraenkel MB, Harris A, Johnson DW, Kesselhut J, Li JJ, Luxton G, Pilmore A, Tiller DJ, Harris DC, Pollock CA (2010) A randomized, controlled trial of early versus late initiation of dialysis. N Engl J Med 363:609–619
14. Evans M, Tettamanti G, Nyren O, Bellocco R, Fored CM, Elinder CG (2011) No survival benefit from early-start dialysis in a population-based, inception cohort study of Swedish patients with chronic kidney disease. J Intern Med 269:289–298
15. Rosansky SJ, Eggers P, Jackson K, Glassock R, Clark WF (2011) Early start of hemodialysis may be harmful. Arch Intern Med 171:396–403

Journal of Neuroscience Research

Journal of Neuroscience Research 90:2163–2172 (2012)

Accumulation of Autofluorescent Storage Material in Brain is Accelerated by Ischemia in Chloride Channel 3 Gene-Deficient Mice

Hirokazu Ohtaki,[1] Kenji Ohara,[1] Dandan Song,[1] Kazuyuki Miyamoto,[1] Tomomi Tsumuraya,[1] Sachiko Yofu,[1,2] Kenji Dohi,[3] Shigeru Tanabe,[4] Sei Sasaki,[5] Shinichi Uchida,[5] Masaji Matsunaga,[2] and Seiji Shioda[1]*

[1]Department of Anatomy, Showa University School of Medicine, Tokyo, Japan
[2]Gene Trophology Research Institute, Tokyo, Japan
[3]Department of Emergency and Critical Care Medicine, Showa University School of Medicine, Tokyo, Japan
[4]Fuji Gotemba Research Laboratories, Chugai Pharmaceutical Co., Ltd., Gotemba, Shizuoka, Japan
[5]Department of Nephrology, Graduate School, Tokyo Medical and Dental University, Tokyo, Japan

Autofluorescent storage material (ASM) is an aging pigment that accumulates during the normal course of senescence. Although the role of ASM has yet to be fully elucidated, ASM has been implicated in age-related neurodegeneration. In this study, we determined the level of ASM in chloride channel 3 (ClC-3) gene-deficient (KO) mice both in response to aging and following mild global ischemia. To understand the mechanism of action of the ASM, mice subjected to ischemia were treated with the cyclooxygenase (COX) inhibitor indomethacin or with the noncompetitive glutamate receptor antagonist MK-801. ClC-3 KO mice displayed age-related neurodegeneration of the neocortex as well as the hippocampus. The cortical layers in particular granular layers became thinner with aging. ASM accumulated in the brains of ClC-3 KO mice was increased seven- to 50-fold over that observed in the corresponding regions of their wild-type littermates. Young wild-type mice survived longer than age-matched ClC-3 KO mice after permanent global ischemia. However, in the case of older animals, the survival curves were similar. The ASM also increased four- to fivefold 10 days after mild global ischemia, an effect that was suppressed by treatment with indomethacin and MK-801. These results suggest that temporary ischemia might trigger a process similar to aging in the brain, mimicking the effect of age-related neurodegenerative diseases.

Key words: aging; autofluorescent storage material; ischemia; chloride channel 3

Autofluorescent storage material (ASM) in the form of lipofuscin is an aging pigment that accumulates during the normal course of senescence. Although the exact role of ASM is not known, it has been implicated in many age-related neurodegenerative diseases, such as Alzheimer's disease (AD) and Parkinson's disease (PD), with amyloid β-protein and/or α-synuclein being identified in the ASM in these conditions (Meredith et al., 2002; Keller, 2006; Seehafer and Pearce, 2006). Another lipofuscin-like ASM, ceroid, is the general term for lipopigment accumulating as a result of a pathological condition. This pigment has also been implicated in neurodegenerative diseases such as neuronal ceroid lipofuscinosis and brain lesions (Seehafer and Pearce, 2006).

Chloride channel 3 (ClC-3) is one of approximately 13 members of the ClC family of voltage-gated chloride ion channels, which have been shown to play diverse roles in various tissues (Koch et al., 1992; Piwon et al., 2000; Bösl et al., 2001; Kornak et al., 2001; Maritzen et al., 2006). ClC-3 is highly expressed in neurons, renal and gastrointestinal epithelial cells, and blood vessels (Lamb et al., 1999; Schmieder et al., 2001). Although ClC-3 is ubiquitously expressed throughout the brain, it is highly expressed in the hippocampus, cerebellum, and olfactory bulb (Kawasaki et al., 1994; Borsani et al., 1995; Stobrawa et al., 2001) and is localized to endosomes and to glutamatergic and GABAergic synaptic vesicles (Stobrawa et al., 2001; Hara-Chikuma et al., 2005). A ClC-3 gene (*clcn3*)-deficient strain of mice (ClC-3 knockout [KO]) was first reported in 2001, and three ClC-3 KO lines have since been generated (Stobrawa et al., 2001; Dickerson et al., 2002; Yoshikawa et al., 2002). Animals deficient in *clcn3* display

Additional Supporting Information may be found in the online version of this article.

Contract grant sponsor: Research on Health Sciences grant focusing on Drug Innovation from The Japan Health Sciences Foundation (to M.M., S.Sh.).

*Correspondence to: Seiji Shioda, PhD, Department of Anatomy, Showa University School of Medicine, 1-5-8 Hatanodai, Shinagawa-Ku, Tokyo 142-8555, Japan. E-mail: shioda@med.showa-u.ac.jp

Received 5 March 2012; Revised 1 May 2012; Accepted 6 June 2012

Published online 30 July 2012 in Wiley Online Library (wileyonlinelibrary.com). DOI: 10.1002/jnr.23110

severe neurodegeneration with aging, particularly in the case of the hippocampus, entorhinal cortex, and photoreceptors. ClC-3 KO mice have also been reported to accumulate lysosome-like structures that mimic the appearance of lipofuscin granules; these granules contain mitochondrial F1F0 ATPase and result in a phenotype that resembles that of cathepsin D KO mice and neuronal ceroid lipofuscinosis (Yoshikawa et al., 2002). Electron microscopic observation revealed that lysosomal-like small droplets could already be detected at postnatal day 12, prior to the appearance of obvious neurodegeneration (Stobrawa et al., 2001).

The vascular hypothesis of AD, first proposed in 1993 (de la Torre and Mussivand, 1993), suggests that impairment of the brain microcirculation might trigger AD (de la Torre, 1994). Cortical hypometabolism and hypoperfusion in PD have also been demonstrated to be risk factors in the progression of that disease (Borghammer et al., 2010). We have previously reported that hypoperfusion induced by global ischemia in the rat resulted in the diffuse spread of neocortical neurodegeneration, particularly in the somatosensory cortex, following delayed neuronal cell death in the hippocampus (Ohtaki et al., 2006a). We have also reported that mitochondrial oxidation increased prior to ischemia-induced neuronal cell death (Ohtaki et al., 2007), with degenerative mitochondrial debris often being demonstrated in association with ASM (Yoshikawa et al., 2002; Seehafer and Pearce, 2006). Furthermore, the accumulation of this material in the heart and brain has been reported following ischemia (Rayment et al., 1999; Wijnen et al., 2002; Ostadalova et al., 2007). However, the relationship between ischemic stress and the accumulation of ASM remains poorly understood.

Here we show that, in ClC-3 KO mice, an increase in the level of ASM occurs in both the hippocampus and the neocortex concomitantly with the development of neurodegeneration. Our results also demonstrate that, whereas young ClC-3 KO mice are more vulnerable to ischemic stress than their wild-type (ClC-$3^{+/+}$) littermates, older wild-type mice display ischemic vulnerability similar to that seen in ClC-3 KO mice. Finally, we reveal that the drastic increase in ASM observed in the ClC-3 KO neocortex following mild ischemia can be suppressed by treatment with indomethacin or MK-801.

MATERIALS AND METHODS

Animals

All experimental procedures involving animals were approved by the Institutional Animal Care and Use Committee of Showa University (Nos. 04094 and 05088). ICR mice with *clcn3* gene disruption (ClC-3 KO) have been described previously (Yoshikawa et al., 2002). All wild-type (ClC-$3^{+/+}$) mice were littermates from the breeding of *clcn3* heterozygous (ClC-$3^{+/-}$) mice in the specific pathogen-free animal facility at Showa University. Animals were maintained on a 12-hr light/dark cycle and had free access to food and water.

Common Carotid Artery Occlusion and Chemical Treatment

ClC-3 KO and wild-type mice were subjected to forebrain ischemia by common carotid artery occlusion (CCAO; Ohtaki et al., 2005, 2008; Inoue et al., 2007). In the first set of experiments, the mice were anesthetized by inhalation of 4.0% sevoflurane, then maintained on 2.5% sevoflurane in N_2O/O_2 (70/30%) through a facemask. Body temperature was monitored with a rectal thermometer and maintained at 37.0–38.0°C using a heating blanket. The common carotid artery (CCA) was carefully exposed bilaterally through a midline incision of the neck and isolated without disrupting the circulation. Both CCAs were tightly double-ligated with 4-0 silk, before being cut to create permanent CCAO (pCCAO). The animals were then taken off anesthetic and kept at room temperature to compare their vulnerability to ischemic stress.

In another set of experiments, ClC-3 KO mice approximately 80 days of age were anesthetized as described above and CCAs occluded with clips (Zen temporary clip; Oowatsusho, Tokyo, Japan). The animals were then taken off anesthetic and kept at room temperature for 8 min, after which they were reanesthetized and the clips were removed to allow restoration of the circulation, resulting in only transient CCAO (tCCAO). The ICR strain of mice is known to have better patency of the posterior communicating artery than C57/BL6 mice (Yang et al., 1997; Kitagawa et al., 1998), and the 8 min tCCAO is considered a period sufficiently short not to induce obvious neuronal cell death, even in the case of the latter strain (Ohtaki et al., 2006b).

When appropriate, indomethacin (5 mg/kg; Sigma, St. Louis, MO) or MK-801 (2 mg/kg; Wako, Osaka, Japan) was dissolved in sterile 0.9% NaCl (saline) and injected interperitoneally (i.p.) immediately after tCCAO, then once daily for 5 (indomethacin) or 2 (MK-801) days. Control animals were given the same volume of saline.

Immunohistochemistry

Mice were anesthetized with sodium pentobarbital (50 mg/kg, i.p.) and perfused transcardially with saline, followed by 4% paraformaldehyde in 50 mM phosphate buffer (pH 7.2). Brains were then removed, postfixed, and cryoprotected in 20% sucrose. Sections were cut on a cryostat at a thickness of 8 μm.

For ClC-3 immunostaining, the sections were preincubated in Dako Protein Block Serum-Free (Dako, Glostrup, Denmark) after quenching endogenous peroxidase with 0.3% H_2O_2. They were then incubated overnight with a polyclonal rabbit anti-ClC-3 primary antibody (1:400; Alomone, Jerusalem, Israel), before being rinsed and incubated with biotinylated horse anti-rabbit IgG (1:200; Santa Cruz Biotechnology, Santa Cruz, CA), followed by an avidin-biotin complex solution (Vector, Burlingame, CA), with diaminobenzidine (DAB; Vector) used as a chromogen. Specificity of the antibody was determined by incubating tissue with and without primary antibodies or by incubating with primary antibodies and a 50-fold amount of ClC-3 antigen (Alomone). Sections were counterstained with hematoxylin after DAB reaction to identify the nuclei.

Fluorescence immunostaining was performed by treating sections with mouse anti-NeuN, a neuronal marker (1:1,000;

Chemicon, Temecula, CA); rabbit anti-GFAP, an astroglial marker (1:20; Dako); and/or rat anti-CD11b, a microglial marker (1:500; AbD Serotec, Oxford, United Kingdom), which were then detected using appropriate Alexa-labeled secondary antibodies (1:400; Invitrogen, Carlsbad, CA). The pattern of immunolabeling was observed with the aid of a fluorescence microscope (Olympus AX-70; Olympus, Tokyo, Japan).

Histology

Anesthetized mice were perfused transcardially with 10% neutral buffered formalin after saline perfusion. Brains were then removed and prepared in a paraffin block. Coronal sections were cut on a microtome at a thickness of 4 μm. Coronal brain sections at approximately 0 mm relative to bregma were used for histological staining as described below. Neuronal cell death and apoptosis-like cell death were detected by Fluoro-Jade B (FJB; Chemicon) staining and in situ terminal deoxynucleotidyl transferase-mediated dUTP nick end labeling (TUNEL) staining. To observe morphological changes in the cortical layers, toluidine blue (TB) staining was performed. FJB and TB staining were carried out according to previous studies (Schmued and Hopkins, 2000; Inoue et al., 2007). TUNEL staining (In Situ Cell Death Detection Kit, POD; Roche, Manheim, Germany) was performed according to the manufacturer's instructions, with minor modifications (Matsunaga et al., 2003). After TUNEL staining, the sections were counterstained with hematoxylin.

Detection of ASM

It has been reported that ASM could be detected as a yellow pigment under brightfield illumination; this material also exhibits autofluorescence, which is excited at 320–480 nm (Seehafer and Pearce, 2006; Kelly et al., 2009; Jung et al., 2010). These characteristics were used to identify the ASM in the present experiments. Preliminary fluorescence microscopy observations carried out with a fluorescence microscope (Olympus AX-70) revealed that the ASM could be detected using a DAPI filter, but only sparingly with FITC and Cy3 filters (Supp. Info. Fig. 1).

The ASM in paraffin-embedded sections was semiquantified in four areas (two areas/hemisphere) of motor to somatosensory cortex 0 mm and −2 mm from bregma and/or two areas of the CA1 sector and dentate gyrus (DG) of the hippocampus at −2 mm relative to bregma. All images were taken with a ×40 objective and corrected for background fluorescence (shadow input level 210, gamma 0.38, highlight input level 255) in Photoshop CS4. The bright autofluorescence was quantified in Scion Image 4.0.3 (http://www.scioncorp.com/) following reversal of the white and black image pixels and expressed as a percentage of the area in the field.

Measurement of Regional Cerebral Blood Flow

Regional cerebral blood flow (rCBF) in the cerebrum of ClC-3 KO and wild-type mice (five animals in each case) was measured before and after CCAO by using a laser-Doppler perfusion imager (PeriScan PIMII; Perimed, Järfälla, Sweden). The laser probe (0.1 mm diameter) of the scanning imager was centered between bregma and lambda, 14 cm above the skull. The scanning area and time were 27 × 27 mm and 49 sec, respectively. In brief, mice were placed in a prone position under 2.5% sevoflurane inhalation, and the skin of the scalp was removed via a midline incision. The rCBF before CCAO was determined by scanning to give a baseline control value (100%). The animals were then subjected to CCAO, after which they were again placed in a prone position, and the rCBF was scanned every 2.5 min for 35 min during ischemia. The rCBF in the cerebrum was obtained at 18–21 points from each hemisphere (total 36–42 points) and calculated as a percentage of the control value.

Statistical Analysis

Data are expressed as mean ± SEM. Statistical comparisons were made by Student's *t*-test for two groups and by one-way ANOVA followed by Dunnett's post hoc tests for multiple groups. $P < 0.05$ was considered statistically significant. Kaplan-Meier survival analysis was used to compare the post-pCCAO survival rates of ClC-3 KO and wild-type mice.

RESULTS

Clinical Symptoms in ClC-3 KO Mice With Aging

Three lines of ClC-3 KO mice have been reported to date (Stobrawa et al., 2001; Dickerson et al., 2002; Yoshikawa et al., 2002), all of which have been shown to display relatively low body weight and degeneration of neurons in the hippocampus, entorhinal cortex, and photoreceptors. We also found that the ClC-3 KO mice have a shorter life span, resulting in an 80% survival rate at approximately 280 days of age (Fig. 1A). Consistent with previous reports, these animals also have a lower body and brain weight (Fig. 1B–D). In particular, the size and weight of the cerebrum were significantly less than those of their wild-type littermates from 93 days of age, whereas significant differences in the weight of cerebellum were also noted at 132 days.

Expression of ClC-3 in the Brain

We next used immunohistochemistry to investigate ClC-3 expression in several regions of the brains of wild-type mice. ClC-3 antibody specificity first was characterized. Dark-brown DAB reaction product in the hippocampal CA1 region was mostly absorbed in the presence of a 50-fold amount of ClC-3 antigen or did not increase in primary antibody-free controls (Fig. 2A–C). Immunoreactivity was subsequently studied in other brain regions. Typical, and mostly neuronal, morphologically ClC-3-immunopositive cells were observed in the CA1 sector of the hippocampus, the neocortex, and the Purkinje and granular cell layers of the cerebellum (Fig. 2J–L). A comparison of the immunoreactivity present in these regions in animals 10, 40, and 80 days of age showed that there was little change in the intensity of labeling in the CA1 region (Fig. 2D–F) or the somatosensory cortex (Fig. 2G–I) with aging.

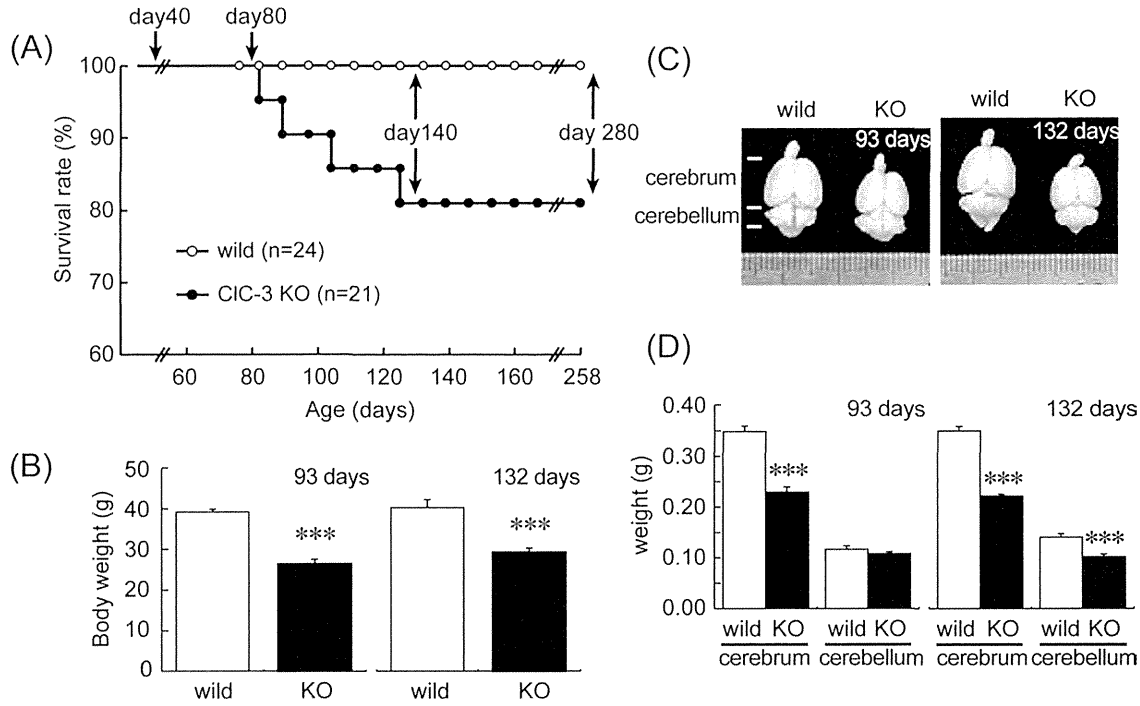

Fig. 1. Comparison of clinical observations in ClC-3 KO mice and their wild-type littermates with aging. ClC-3 KO mice display higher mortality with aging (**A**) and lower body weight (**B**) than their wild-type littermates. Representative macroscopic images (**C**) and weights (**D**) for ClC-3 KO and wild-type mice. Data are expressed as mean ± SEM (n = 8). ***$P < 0.001$ vs. wild-type mice (Student's *t*-test).

Neocortical Degeneration in ClC-3 KO Mice

It has been reported that hippocampal and entorhinal cortical neurons degenerate in ClC-3 KO mice (Stobrawa et al., 2001; Dickerson et al., 2002; Yoshikawa et al., 2002). We observed a motor to somatosensory cortical neurodegeneration consistent with those previous reports. Unlike the case in wild-type animals, a significant number of FJB-positive cells was observed in the neocortex of the ClC-3 KO mice, an effect that increased with aging (Fig. 3A). Furthermore, the labelled cells were not randomly distributed in cortical regions but rather occurred in some specific layers. Immunostaining of brain sections with the neuronal marker NeuN was carried out to identify degenerating cortical layer cells in the ClC-3 KO mice (Fig. 3B). Five or six cortical layers were identified in 40-day-old wild-type animals. In age-matched ClC-3 KO mice, these layers were thinner, with only a small number of NeuN-positive cells observed in layer IV. The overall thickness of the cortical layers gradually decreased with age, with the small granular neurons in cortical layers II + III and IV being particularly affected (Fig. 3C). At 80 days of age, TUNEL-positive cells were also observed in cortical layers II + III and IV of ClC-3 KO mice. A morphological study using TB staining showed that the number of neuronal cells in cortical layers, particularly cortical layers II–IV, of 140-day-old ClC-3 KO mice diminished considerably compared with wild-type controls, and the nuclei and nucleolus were unclear. Although the cortical layer became thinner, vacuolation was not evident (Fig. 3D). Moreover, colabeling for NeuN, GFAP, and CD11b revealed numerous astroglial and microglial cells in the same layers, suggesting that gliosis had been induced (Fig. 3E).

Accumulation of ASM With Aging

ClC-3 KO mice are known to accumulate lysosome-like lipid droplets in the brain (Stobrawa et al., 2001; Yoshikawa et al., 2002). These droplets resemble lipofuscin granules in neuronal cells and have been observed at the electron microscopic level in 6-week-old mice.

We first characterized the deposits using brightfield illumination after H&E staining of slices. It was difficult to observe the presence of clear yellow pigment in the brains of 6-week-old mice (40 days), but such pigment was plainly evident in the hippocampal region of 80-day-old mice and was accompanied by severe neuronal cell death (Fig. 4A). When a fluorescence microscope fitted with a DAPI filter was used to observe the yellow pigment, the pigment autofluoresced in its entirety (Fig. 4B). These findings were a typically consistent feature of ASM such as lipofuscin and ceroid. Moreover, the ASM

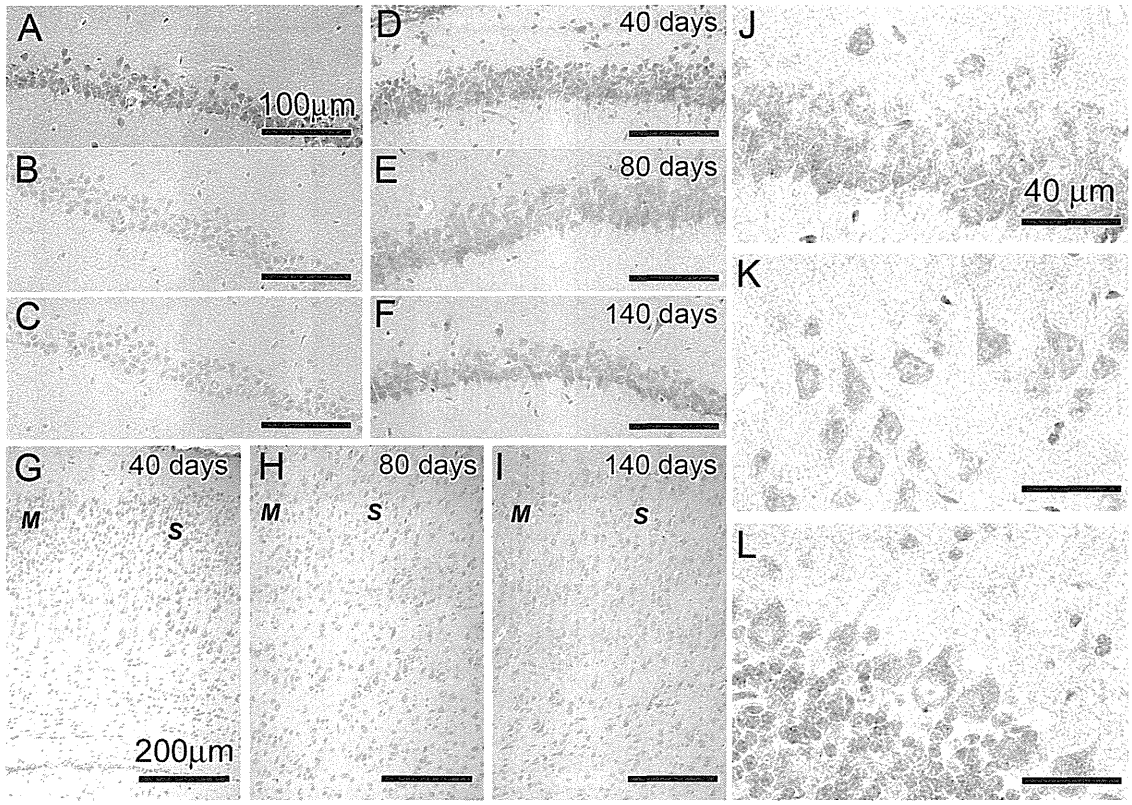

Fig. 2. ClC-3 immunoreactivity in the wild-type brain. A–C: Characterization of the anti-ClC-3 antibody, with dark-brown DAB reaction product observed in the CA1 sector of the hippocampus (**A**). The reaction product is absorbed by incubating primary antibodies and a 50-fold amount of ClC-3 antigen (**B**) or is decreased in primary antibody-free control (**C**). ClC-3 immunoreactivity is observed in neuronal cells of the hippocampus (**D–F,J**), motor (M) to somatosensory (S) cortex at bregma 0 ± 0.5 mm (**G–I,K**), and cerebellum (**L**). The ClC-3 immunoreactivity in the hippocampus (D–F) and neocortex (G–I) is compared with different ages. Scale bars = 100 μm in A (applies to A–F); 200 μm in G (applies to G–I); 40 μm in J (applies to J–L). [Color figure can be viewed in the online issue, which is available at wileyonlinelibrary.com.]

was more sensitive to detection by fluorescence microscopy than by brightfield illumination.

Changes in the content of ASM with aging (at 40, 80, and 140 days of age) were then semiquantified in the CA1 sector and the dentate gyrus (DG) of the hippocampus as well as in the somatosensory cortex (Fig. 4C–F). In these regions, in 40-day-old wild-type mice (n = 5–6), the material occupied from 0.007% to 0.018% of the area. Values in ClC-3 KO mice were 0.80% ± 0.20%, 0.62% ± 0.25%, 0.07% ± 0.04%, and 0.08% ± 0.04% in CA1, DG, and 0 mm and −2 mm relative to bregma in the somatosensory cortex, respectively. The ASM in the CA1 sector of hippocampus in the ClC-3 KO did not show a further increase with aging, suggesting that the CA1 region at 40 days in ClC3 KO mice has already degenerated severely (Supp. Info. Fig. 2) and that the accumulation of ASM might already be saturated. However, other regions showed further significant increases with aging, resulting in values of 1.18% ± 0.50%, 0.42% ± 0.21%, and 0.35% ± 0.17% in the DG and 0 mm and −2 mm from bregma in the somatosensory cortex in 140-day-old mice. The ASM in wild-type mice also increased with aging, although to a lesser extent than in the ClC-3 KO animals, the corresponding values being 0.19% ± 0.24%, 0.03% ± 0.02%, 0.07% ± 0.04%, and 0.08% ± 0.04% in CA1, DG, and 0 mm and −2 mm from bregma, respectively, at 140 days. The ASM in the cortical regions at 140 days in wild-type mice was significantly greater than that at 40 days.

Vulnerability of ClC-3 KO Mice to Ischemic Stress

We have previously reported that hypoperfusion by pCCAO in Wistar rats causes neuronal cell death first in the hippocampus within 1 week and then more diffusely in the cerebral cortex over a period of 4 weeks (Ohtaki et al., 2006a). This progressive pattern of neuronal cell death is similar to the phenotype observed in ClC-3 KO mice, so we hypothesized that these mice might be vulnerable to ischemic stress. To investigate this, two age groups of ClC-3 KO mice and their wild-type littermates were subjected to pCCAO (Fig. 5A). Young ClC-3 KO mice (129 ± 1.7 days old, n = 25) had a 50% survival time of 11 min 14 sec (11′14″), whereas their wild-type counterparts (132 ± 2.4 days old, n = 35) survived significantly longer (50% survival time of 18′08″; $P < 0.05$ by Kaplan-Meier survival analysis).

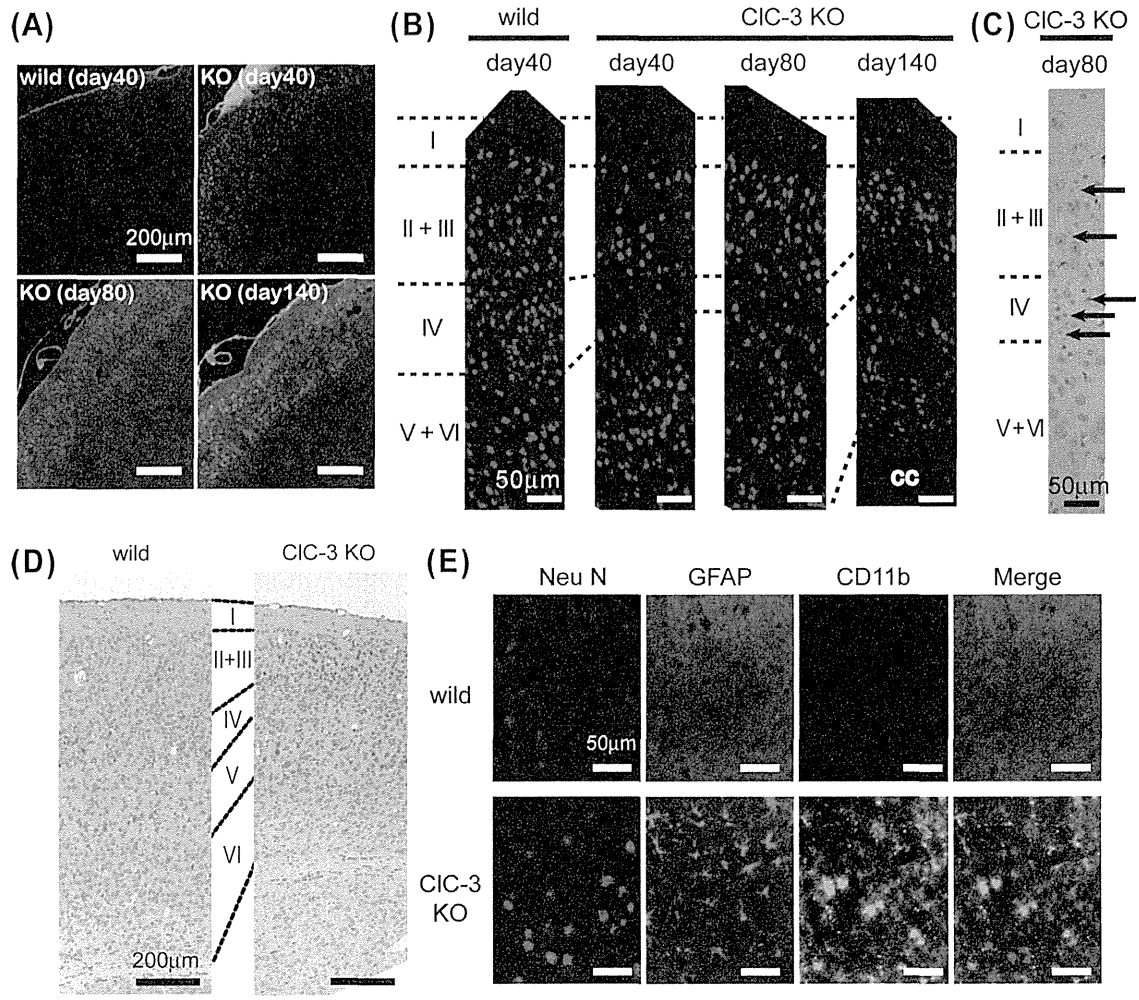

Fig. 3. Progressive neuronal cell death is observed in the neocortex of ClC-3 KO mice. **A**: Fluoro-Jade B (FJB) staining reveals neurodegeneration in the motor to somatosensory regions of the neocortex of 40-day-old ClC-3 KO (KO) mice, but not their wild-type (wild) littermates. This FJB labeling increases with aging. **B**: Immunolabeling with the neuronal marker NeuN reveals that the neocortical layers, in particular layers II + III and IV, shrink with aging in the ClC-3 KO mice. The corpus callosum is indicated as cc. **C**: TUNEL-positive cells are clearly observed in cortical layers II + III and IV of 80-day-old ClC-3 KO mice (arrows). **D**: Morphological comparison of 140-day-old brain slices shows that the cortical layers, in particular cortical layers II–IV, of ClC-3 KO mice undergo shrinking and that the total cortical layer becomes thinner. **E**: Astro- and microgliosis are also apparent in the same layers at this time point, unlike the case in age-matched wild-type ($ClC^{+/+}$) mice. Scale bars = 200 μm in A,D; 50 μm in B,C,E. [Color figure can be viewed in the online issue, which is available at wileyonlinelibrary.com.]

The rCBF during ischemia was not significantly different between the two groups during the 35 min following pCCAO (Fig. 5B,C), suggesting that *clcn3* deficiency or the accumulation of ASM was responsible for the ischemic vulnerability of the ClC-3 KO mice.

ClC-3 KO mice aged 278 ± 3.2 days (n = 16) presented a survival curve similar to that of the corresponding younger animals, with a 50% survival of 12′30″. In contrast, the survival curve in older wild-type mice (275 ± 2.9 days old, n = 24) differed from that of their younger counterparts, more closely resembling that of ClC-3 KO mice (50% survival time of 11′34″). These results suggested that ASM accumulation or age-dependent phenomena could underpin the vulnerability to ischemic stress.

Increase in ASM After tCCAO

To determine the relationship between ischemia and ASM, approximately 80-day-old ClC-3 KO mice were subjected to mild tCCAO. In this experiment, the CCAs of mice were clipped for the relatively short period of 8 min, which we expected would induce either no neuronal cell death or at least less than that described from previous studies (Yang et al., 1997; Kitagawa et al., 1998; Ohtaki et al., 2006b). After CCAO, the ASM was semiquantified in the somatosensory cortex 0 and −2 mm relative to bregma over a period of 10 days (Fig. 6). There was no significant increase in ASM in animals that were not subjected to tCCAO (data not shown). Little change in the ASM was detected in the somato-

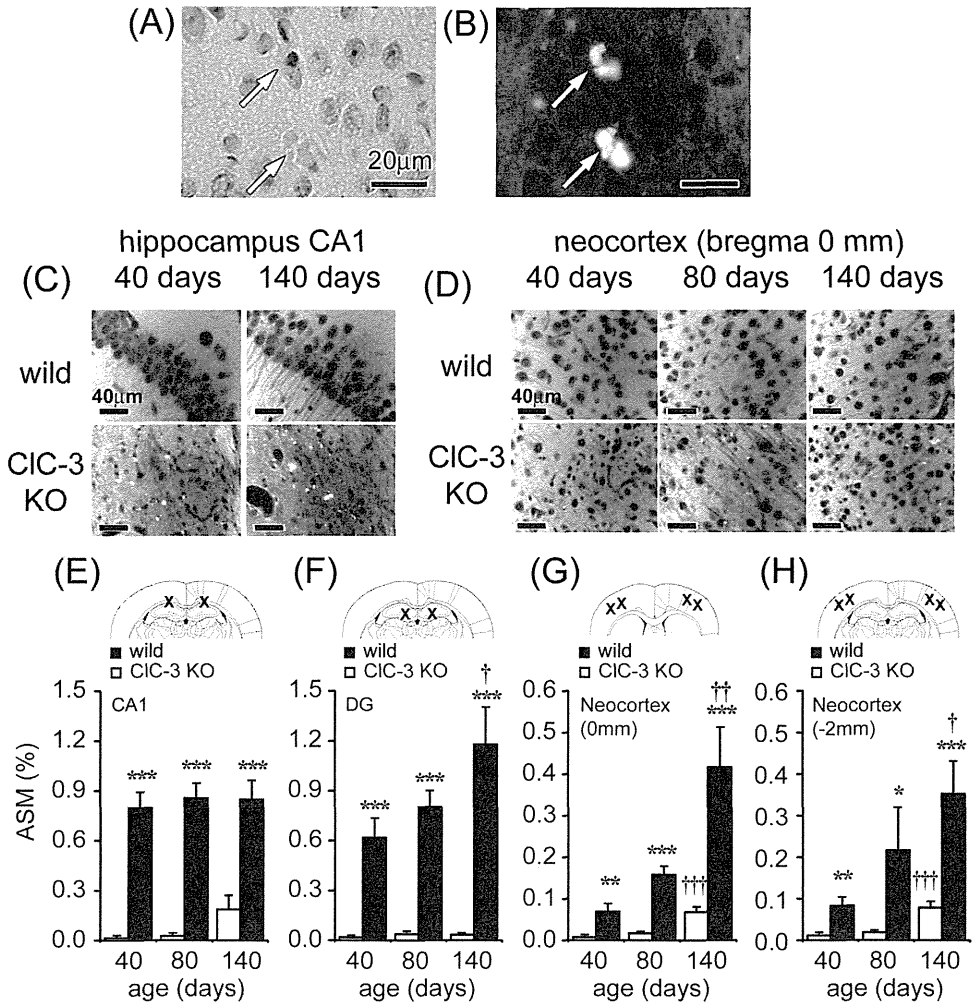

Fig. 4. Comparison of autofluorescent storage material (ASM) in ClC-3 KO and wild-type mice with aging. **A**: ASM, which is characterized as a yellow pigment (arrow) under brightfield illumination, is detected in the hippocampus of 80-day-old CLC-3 KO mice. **B**: This material also autofluoresces (arrow), as illustrated in the same sections as in A. Representative images of ASM in hippocampal CA1 region (**C**) and at 0 mm from bregma in the neocortex (**D**). Images of brain sections from ClC-3 KO mice also showed considerable bright ASM. Semi-quantification of the ASM was performed for the hippocampal CA1 (**E**), dentate gyrus (DG; **F**), and 0 (**G**) and −2 (**H**) mm from bregma in the motor to somatosensory cortex with aging (n = 5–9). The area used for quantification (crosses) is indicated in the **insets** in E–H. Data are expressed as mean ± SEM. $*P < 0.05$, $**P < 0.01$, $***P < 0.001$ vs. age-matched wild-type mice (Student's *t*-test). $\dagger P < 0.05$, $\dagger\dagger P < 0.01$, $\dagger\dagger\dagger P < 0.001$ vs. percentage of ASM (%) at 40 days of age for each genotype (Dunnet post hoc test). Scale bars = 20 μm in A (applies to A,B); 40 μm in C,D. [Color figure can be viewed in the online issue, which is available at wileyonlinelibrary.com.]

sensory cortex over the first 5 days following tCCAO. However, after 10 days, a four- to fivefold increase in ASM content was observed in this region ($P < 0.001$; Fig. 6D–F,I). In contrast, considerable amounts of ASM were already apparent in the CA1 sector of the hippocampus prior to ischemia, with little change in the level observed following tCCAO (Fig. 6A–C).

To determine which ischemic pathway contributed to the accumulation of ASM, the mice were treated with indomethacin, a pan-cyclooxygenase (COX) inhibitor, or with MK-801, an antagonist of the N-methyl-D-aspartate (NMDA) receptor, the latter being a member of the glutamate family of receptors (Fig. 6G–I). Both indomethacin and MK-801 treatment significantly reduced the level of ASM observed in the somatosensory cortex, suggesting that ischemic stress influences the accumulation of ASM.

DISCUSSION

ASM is an aging pigment that accumulates in neurons during the normal course of senescence. ASM deposits often contain amyloid β-protein and/or α-synuclein, so this material has been implicated as a contributor to AD and PD (Meredith et al., 2002; Keller, 2006; Seehafer and Pearce, 2006). We therefore investigated aspects of the accumulation of ASM with aging and under ischemic stress to understand the mechanisms the accumulation of this material in ClC-3 KO mice.

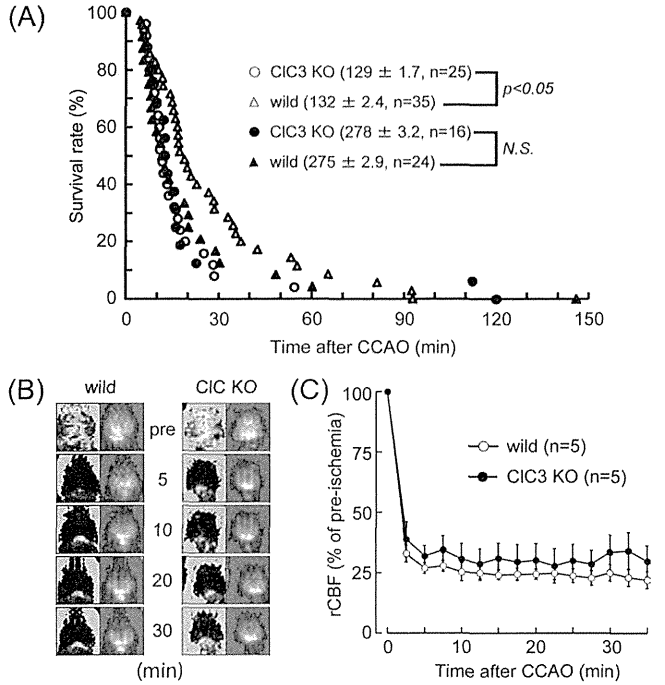

Fig. 5. ClC-3 KO mice are vulnerable to ischemic stress. **A**: ClC-3 KO and wild-type (wild) mice were subjected to pCCAO. Young ClC-3 KO mice (129 ± 1.7 days old) are more vulnerable to ischemic stress than their age-matched wild-type littermates (132 ± 2.4 days old). However, older wild-type animals (275 ± 2.9 days old) are as vulnerable as ClC-3 KO mice (278 ± 3.2 days old). **B,C**: Level of rCBF in ClC-3 KO (ClC KO) and wild-type (wild) mice after CCAO. B: Representative images of rCBF before and for 30 min after CCAO. After ischemia, the rCBF drastically decreases in the cerebrum, with less of a reduction observed in the cerebellum. C: Quantification of rCBF after CCAO; no significant differences are recorded (Student's *t*-test). [Color figure can be viewed in the online issue, which is available at wileyonlinelibrary.com.]

ClC-3 KO mice were used here as they displayed a phenotype to increase the ASM and to undergo heightened neuronal cell death in the hippocampus. ClC-3 KO mice had low body weights and high rates of mortality as well as progressive brain shrinkage. These characteristics were consistent with the findings from previous studies (Stobrawa et al., 2001; Dickerson et al., 2002; Yoshikawa et al., 2002). To determine the distribution of ClC-3 in the brain with aging, ClC-3 immunoreactivity was widely observed in the hippocampus, neocortex and cerebellum of wild-type mice. We then investigated neurodegeneration with aging in ClC-3 KO mice and observed neuronal cell death in the neocortex, in addition to the hippocampus and entorhinal cortex, although the former progressed relatively slowly in comparison with that observed in the hippocampus. Neurodegeneration in the neocortex was recognized in specific cortical layers, in the motor to somatosensory cortical layers, and in particular the small, presumably granular neurons of layers II + III and IV, became progressively compromised. Although we did not identify what kinds of neurons degenerated in ClC-3 KO mice, Dickerson et al. (2002) reported that GABAergic neurons were influenced in ClC-3 KO mice, and the ClC-3 KO mice exhibited an epileptic phenotype. Semiquantification of the ASM in the hippocampus and motor to somatosensory cortex of the ClC-3 KO and wild-type mice with aging showed that this material was clearly present in the CA1 sector of the hippocampus of ClC-3 KO mice, even though levels did not increase dramatically with aging. This result was expected because lysosome-like structures, which probably develop into ASM within the hippocampus, were already apparent in ClC-3 KO mice by postnatal day 7, and the neuronal layers and the structure of the hippocampus of these animals break down by 6 weeks of age (Stobrawa et al., 2001; Yoshikawa et al., 2002). These findings suggest that the accumulation of ASM might be closely involved in the induction of neuronal cell death. However, we also found that levels of ASM in the neocortex of the ClC-3 KO mice progressively increased with aging, a finding that was reflected in wild-type mice, although levels of the material in wild-type mice were significantly lower than the level in the KO mice, without any apparent neuronal cell death.

We next determined whether the accumulation of ASM influenced the vulnerability of the mice to ischemic stress at different ages. Young and old ClC-3 KO mice showed a similar survival curve after pCCAO, whereas young wild-type mice survived significantly longer. Because the rCBF did not differ between the young ClC-3 KO and wild-type animals, we concluded that the latter group might be more resilient to ischemic stress. Interestingly, however, the survival curve in older wild-type mice was similar to that of the ClC-3 KO animals. This led us to hypothesize that an age-related substance, possibly ASM, might contribute to ischemic vulnerability.

Impairment of brain microcirculation is considered to be a trigger and a risk factor in the progression of AD, PD, vascular dementia, and other neurodegenerative diseases (Kawamura et al., 1991; de la Torre and Mussivand, 1993; de la Torre, 1994; Meyer et al., 1995; Shyu et al., 1996; Hanyu et al., 2004; Borghammer et al., 2010). We have previously reported that chronic hypoperfusion induced by global ischemia in the rat caused progressive cortical neural cell death following initial hippocampal cell death, a neurodegenerative pattern similar to that observed in the ClC-3 KO mice (Ohtaki et al., 2006a). This led us to postulate that ischemic stress might influence ASM accumulation in the brain, prompting us to investigate the outcome of mild tCCAO in these animals. In an attempt to elucidate the underlying mechanism, we also examined the effect of pharmacological agents that have been reported to prevent ischemic neural cell death, in line with previous studies demonstrating that accumulation of ASM occurs in the heart and brain following ischemia (Rayment et al., 1999; Wijnen et al., 2002; Ostadalova et al., 2007). Neocortical accumulation of ASM was significantly increased 10 days after mild tCCAO, whereas no

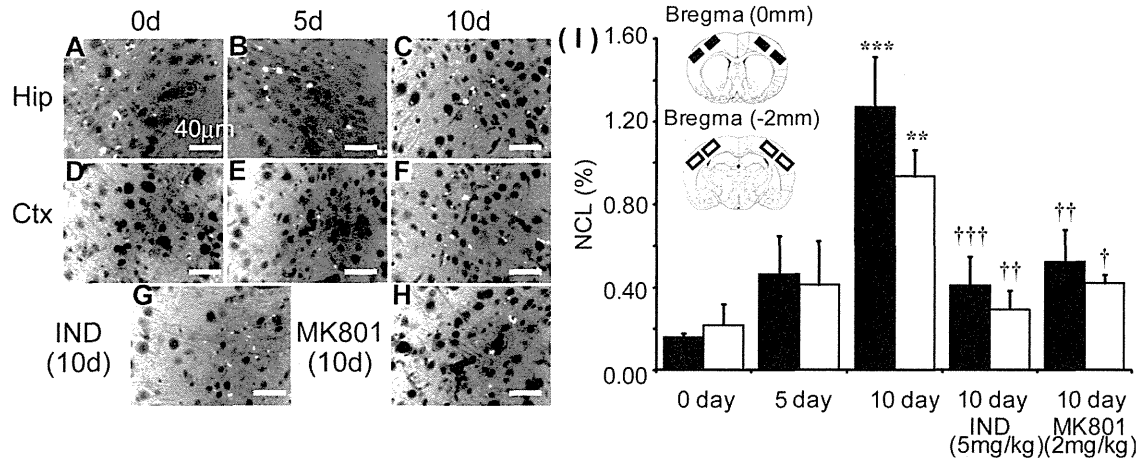

Fig. 6. Ischemic stress accelerates the accumulation of ASM in the brain. Representative images of the ASM in the hippocampus (Hip; **A–C**) and neocortex 0 mm from bregma (Ctx; **D–H**) at 0 (nonischemic control; A,D), 5 (B,E), and 10 (C,F–H) days after mild tCCAO. The ASM significantly increases in the neocortex (D–F,I) 10 days after tCCAO, but no such effect is observed in the CA1 sector of the hippocampus (A–C). Injections of indomethacin (IND; 5 mg/kg; G) or MK801 (2 mg/kg; H) led to a reduction in the level of ASM. Indomethacin treatment significantly decreases ASM accumulation at 10 days (**I**). Semiquantification of ASM was performed, with the area indicated by open and solid boxes in the **insets**. Data are expressed as the mean ± SEM (n = 4–6). $^{**}P < 0.01$, $^{***}P < 0.001$ vs. nonischemic control mice (Dunnet's post hoc test). $\dagger P < 0.05$, $\dagger\dagger P < 0.01$, $\dagger\dagger\dagger P < 0.001$ vs. 10-day ischemic animals (Dunnet's post hoc test). Scale bar = 40 μm.

significant difference was recorded at 5 days. Interestingly, this ASM accumulation was significantly suppressed by treatment with indomethacin or MK-801, clearly indicating that a series of stress-related events following mild ischemia accelerates ASM accumulation and suggesting that lipid metabolism involving COX and/or oxidative stress may contribute to this progression. The results also suggest that even temporary hypoperfusion might accelerate the aging process in the brain, increasing the likelihood of developing an age-related neurodegenerative disease.

Several issues must be addressed before we can conclude that temporary ischemia or hypoperfusion by stenosis can directly induce neurodegenerative disease or whether prevention of ASM accumulation can exert a protective effect. ClC-3 KO mice are unable to facilitate acidification of the endosome/lysosome pathway, thereby impairing liposomal function (Li et al., 2002; Hara-Chikuma et al., 2005). Recently, it has been reported that acidification of lysosomes in microglial cells is involved in amyloid fibril degradation. Impairment of lysosomal acidification increased amyloid fibrils, with another ClC family member, ClC-7, required for the acidification (Majumdar et al., 2011). Another study also suggested that presenilin-1 (PS-1) was required for lysosomal proteolysis and autophagy and that these functions were disrupted in PS-1 mutant mice, which exhibit AD-like behavior (Lee et al., 2010). ClC-3 is located in the endosomal/lysosomal membrane and contributes to the acidification and degradation of ASM. These findings suggest that *clcn3* deficiency, lysosomal impairment, and/or ischemic stress (hypoperfusion), which increases ASM accumulation, might be involved in the induction of neurodegenerative diseases, whereas the improvement of cerebral circulation or inhibition of ischemic stress signaling might reduce the risk of neurodegenerative diseases. Further studies are therefore needed to clarify both the commonalities and the points of difference between ASM accumulation and the development of neurodegenerative disease.

REFERENCES

Borghammer P, Chakravarty M, Jonsdottir K, Sato N, Matsuda H, Ito K, Arahata Y, Kato T, Gjedde A. 2010. Cortical hypometabolism and hypoperfusion in Parkinson's disease is extensive: probably even at early disease stages. Brain Struct Funct 214:303–317.

Borsani G, Rugarli E, Taglialatela M, Wong C, Ballabio A. 1995. Characterization of a human and murine gene (CLCN3) sharing similarities to voltage-gated chloride channels and to a yeast integral membrane protein. Genomics 27:131–141.

Bösl M, Stein V, Hübner C, Zdebik A, Jordt S, Mukhopadhyay A, Davidoff M, Holstein A, Jentsch T. 2001. Male germ cells and photoreceptors, both dependent on close cell–cell interactions, degenerate upon ClC-2 Cl^- channel disruption. EMBO J 20:1289–1299.

de la Torre J. 1994. Impaired brain microcirculation may trigger Alzheimer's disease. Neurosci Biobehav Rev 18:397–401.

de la Torre J, Mussivand T. 1993. Can disturbed brain microcirculation cause Alzheimer's disease? Neurol Res 15:146–153.

Dickerson L, Bonthius D, Schutte B, Yang B, Barna T, Bailey M, Nehrke K, Williamson R, Lamb F. 2002. Altered GABAergic function accompanies hippocampal degeneration in mice lacking ClC-3 voltage-gated chloride channels. Brain Res 958:227–250.

Hanyu H, Shimuzu S, Tanaka Y, Takasaki M, Koizumi K, Abe K. 2004. Cerebral blood flow patterns in Binswanger's disease: a SPECT study using three-dimensional stereotactic surface projections. J Neurol Sci 220:79–84.

Hara-Chikuma M, Yang B, Sonawane N, Sasaki S, Uchida S, Verkman A. 2005. ClC-3 chloride channels facilitate endosomal acidification and chloride accumulation. J Biol Chem 280:1241–1247.

Inoue H, Ohtaki H, Nakamachi T, Shioda S, Okada Y. 2007. Anion channel blockers attenuate delayed neuronal cell death induced by transient forebrain ischemia. J Neurosci Res 85:1427–1435.

Jung T, Höhn A, Grune T. 2010. Lipofuscin: detection and quantification by microscopic techniques. Methods Mol Biol 594:173–193.

Kawamura J, Meyer JS, Terayama Y, Weathers S. 1991. Cerebral hyperemia during spontaneous cluster headaches with excessive cerebral vasoconstriction to hyperoxia. Headache 31:222–227.

Kawasaki M, Uchida S, Monkawa T, Miyawaki A, Mikoshiba K, Marumo F, Sasaki S. 1994. Cloning and expression of a protein kinase C-regulated chloride channel abundantly expressed in rat brain neuronal cells. Neuron 12:597–604.

Keller J. 2006. Age-related neuropathology, cognitive decline, and Alzheimer's disease. Ageing Res Rev 5:1–13.

Kelly J, Weiss A, Rowell G, Seigel G. 2009. Autofluorescence and infrared retinal imaging in patients and obligate carriers with neuronal ceroid lipofuscinosis. Ophthalmic Genet 30:190–198.

Kitagawa K, Matsumoto M, Yang G, Mabuchi T, Yagita Y, Hori M, Yanagihara T. 1998. Cerebral ischemia after bilateral carotid artery occlusion and intraluminal suture occlusion in mice: evaluation of the patency of the posterior communicating artery. J Cereb Blood Flow Metab 18:570–579.

Koch M, Steinmeyer K, Lorenz C, Ricker K, Wolf F, Otto M, Zoll B, Lehmann-Horn F, Grzeschik K, Jentsch T. 1992. The skeletal muscle chloride channel in dominant and recessive human myotonia. Science 257:797–800.

Kornak U, Kasper D, Bösl M, Kaiser E, Schweizer M, Schulz A, Friedrich W, Delling G, Jentsch T. 2001. Loss of the ClC-7 chloride channel leads to osteopetrosis in mice and man. Cell 104:205–215.

Lamb F, Clayton G, Liu B, Smith R, Barna T, Schutte B. 1999. Expression of CLCN voltage-gated chloride channel genes in human blood vessels. J Mol Cell Cardiol 31:657–666.

Lee JH, Yu WH, Kumar A, Lee S, Mohan PS, Peterhoff CM, Wolfe DM, Martinez-Vicente M, Massey AC, Sovak G, Uchiyama Y, Westaway D, Cuervo AM, Nixon RA. 2010. Lysosomal proteolysis and autophagy require presenilin 1 and are disrupted by Alzheimer-related PS1 mutations. Cell 141:1146–1158.

Li X, Wang T, Zhao Z, Weinman S. 2002. The ClC-3 chloride channel promotes acidification of lysosomes in CHO-K1 and Huh-7 cells. Am J Physiol Cell Physiol 282:C1483–C1491.

Majumdar A, Capetillo-Zarate E, Cruz D, Gouras GK, Maxfield FR. 2011. Degradation of Alzheimer's amyloid fibrils by microglia requires delivery of ClC-7 to lysosomes. Mol Biol Cell 22:1664–1676.

Maritzen T, Blanz J, Jentsch T. 2006. Physiological functions of the CLC chloride transport proteins. New York: Elsevier. p 9–57.

Matsunaga M, Ohtaki H, Takaki A, Iwai Y, Yin L, Mizuguchi H, Miyake T, Usumi K, Shioda S. 2003. Nucleoprotamine diet derived from salmon soft roe protects mouse hippocampal neurons from delayed cell death after transient forebrain ischemia. Neurosci Res 47:269–276.

Meredith G, Totterdell S, Petroske E, Santa Cruz K, Callison RJ, Lau Y. 2002. Lysosomal malfunction accompanies alpha-synuclein aggregation in a progressive mouse model of Parkinson's disease. Brain Res 956:156–165.

Meyer JS, Muramatsu K, Mortel KF, Obara K, Shirai T. 1995. Prospective CT confirms differences between vascular and Alzheimer's dementia. Stroke 26:735–742.

Ohtaki H, Dohi K, Nakamachi T, Yofu S, Endo S, Kudo Y, Shioda S. 2005. Evaluation of brain ischemia in mice. Acta Histochem Cytochem 38:99–106.

Ohtaki H, Fujimoto T, Sato T, Kishimoto K, Fujimoto M, Moriya M, Shioda S. 2006a. Progressive expression of vascular endothelial growth factor (VEGF) and angiogenesis after chronic ischemic hypoperfusion in rat. Acta Neurochir Suppl 96:283–287.

Ohtaki H, Nakamachi T, Dohi K, Yofu S, Hodoyama K, Matsunaga M, Aruga T, Shioda S. 2006b. Controlled normothermia during ischemia is important for the induction of neuronal cell death after global ischemia in mouse. Acta Neurochir Suppl 96:249–253.

Ohtaki H, Takeda T, Dohi K, Yofu S, Nakamachi T, Satoh K, Hiraizumi Y, Miyaoka H, Matsunaga M, Shioda S. 2007. Increased mitochondrial DNA oxidative damage after transient middle cerebral artery occlusion in mice. Neurosci Res 58:349–355.

Ohtaki H, Ylostalo J, Foraker J, Robinson A, Reger R, Shioda S, Prockop D. 2008. Stem/progenitor cells from bone marrow decrease neuronal death in global ischemia by modulation of inflammatory/immune responses. Proc Natl Acad Sci U S A 105:14638–14643.

Ostadalova I, Vobecky M, Chvojkova Z, Mikova D, Hampl V, Wilhelm J, Ostadal B. 2007. Selenium protects the immature rat heart against ischemia/reperfusion injury. Mol Cell Biochem 300:259–267.

Piwon N, Günther W, Schwake M, Bösl M, Jentsch T. 2000. ClC-5 Cl^--channel disruption impairs endocytosis in a mouse model for Dent's disease. Nature 408:369–373.

Rayment N, Haven A, Madden B, Murday A, Trickey R, Shipley M, Davies M, Katz D. 1999. Myocyte loss in chronic heart failure. J Pathol 188:213–219.

Schmieder S, Lindenthal S, Ehrenfeld J. 2001. Tissue-specific N-glycosylation of the ClC-3 chloride channel. Biochem Biophys Res Commun 286:635–640.

Schmued L, Hopkins K. 2000. Fluoro-Jade B: a high affinity fluorescent marker for the localization of neuronal degeneration. Brain Res 874:123–130.

Seehafer S, Pearce D. 2006. You say lipofuscin, we say ceroid: defining autofluorescent storage material. Neurobiol Aging 27:576–588.

Shyu WC, Lin JC, Shen CC, Hsu YD, Lee CC, Shiah IS, Tsao WL. 1996. Vascular dementia of Binswanger's type: clinical, neuroradiological and ^{99}mTc-HMPAO SPET study. Eur J Nucl Med 23:1338–1344.

Stobrawa S, Breiderhoff T, Takamori S, Engel D, Schweizer M, Zdebik A, Bösl M, Ruether K, Jahn H, Draguhn A, Jahn R, Jentsch T. 2001. Disruption of ClC-3, a chloride channel expressed on synaptic vesicles, leads to a loss of the hippocampus. Neuron 29:185–196.

Wijnen M, Roumen R, Vader H, Goris R. 2002. A multiantioxidant supplementation reduces damage from ischaemia reperfusion in patients after lower torso ischaemia. A randomised trial. Eur J Vasc Endovasc Surg 23:486–490.

Yang G, Kitagawa K, Matsushita K, Mabuchi T, Yagita Y, Yanagihara T, Matsumoto M. 1997. C57BL/6 strain is most susceptible to cerebral ischemia following bilateral common carotid occlusion among seven mouse strains: selective neuronal death in the murine transient forebrain ischemia. Brain Res 752:209–218.

Yoshikawa M, Uchida S, Ezaki J, Rai T, Hayama A, Kobayashi K, Kida Y, Noda M, Koike M, Uchiyama Y, Marumo F, Kominami E, Sasaki S. 2002. CLC-3 deficiency leads to phenotypes similar to human neuronal ceroid lipofuscinosis. Genes Cells 7:597–605.

A minor role of WNK3 in regulating phosphorylation of renal NKCC2 and NCC co-transporters *in vivo*

Katsuyuki Oi[1], Eisei Sohara[1,*], Tatemitsu Rai[1], Moko Misawa[1], Motoko Chiga[1], Dario R. Alessi[2], Sei Sasaki[1] and Shinichi Uchida[1]

[1]Department of Nephrology, Graduate School of Medical and Dental Sciences, Tokyo Medical and Dental University, 1-5-45 Yushima, Bunkyo-ku, Tokyo 113-8519, Japan
[2]MRC Protein Phosphorylation Unit, College of Life Sciences, University of Dundee, Dow Street, Dundee DD1 5EH, Scotland, UK
*Author for correspondence (esohara.kid@tmd.ac.jp)

Biology Open 1, 120–127
doi: 10.1242/bio.2011048

Summary

Mutations in WNK1 and WNK4 kinase genes have been shown to cause a human hereditary hypertensive disease, pseudohypoaldosteronism type II (PHAII). We previously discovered that WNK kinases phosphorylate and activate OSR1/SPAK kinases that regulate renal SLC12A family transporters such as NKCC2 and NCC, and clarified that the constitutive activation of this cascade causes PHAII. WNK3, another member of the WNK kinase family, was reported to be a strong activator of NCC/NKCC2 when assayed in *Xenopus* oocytes, suggesting that WNK3 also plays a major role in regulating blood pressure and sodium reabsorption in the kidney. However, it remains to be determined whether WNK3 is in fact involved in the regulation of these transporters in vivo. To clarify this issue, we generated and analyzed WNK3 knockout mice. Surprisingly, phosphorylation and expression of OSR1, SPAK, NKCC2 and NCC did not decrease in knockout mouse kidney under normal and low-salt diets. Similarly, expression of epithelial Na channel and Na/H exchanger 3 were not affected in knockout mice. Na^+ and K^+ excretion in urine in WNK3 knockout mice was not affected under different salt diets. Blood pressure in WNK3 knockout mice was not lower under normal diet. However, lower blood pressure was observed in WNK3 knockout mice fed low-salt diet. WNK4 and WNK1 expression was slightly elevated in the knockout mice under low-salt diet, suggesting compensation for WNK3 knockout by these WNKs. Thus, WNK3 may have some role in the WNK-OSR1/SPAK-NCC/NKCC2 signal cascade in the kidney, but its contribution to total WNK kinase activity may be minimal.

Key words: Na-K-Cl cotransporter, Na-Cl cotransporter, WNK3, mouse kidney, WNK

Introduction

Pseudohypoaldosteronism type II (PHAII) is an autosomal-dominant disease characterized by hypertension due to increased renal salt reabsorption, hyperkalemia and metabolic acidosis (Gordon, 1986; Schambelan et al., 1981; Achard et al., 2001). Mutations in with-no-lysine kinase 1 (WNK1) and with-no-lysine kinase 4 (WNK4) have been reported to cause PHAII (Wilson et al., 2001). We generated $WNK4^{D561A/+}$ knock-in mice, an ideal mouse model of PHAII, and observed increased phosphorylation of oxidative stress-responsive kinase-1 (OSR1), STE20/SPS1-related proline/alanine-rich kinase (SPAK) and thiazide-sensitive Na-Cl co-transporter (NCC) (Yang, S. S. et al., 2007). We previously demonstrated in in vitro experiments that WNK1 and WNK4 phosphorylated and activated OSR1 and SPAK kinases, and that OSR1 and SPAK could phosphorylate NCC (Moriguchi et al., 2005; Vitari et al., 2005; Vitari et al., 2006; Richardson et al., 2008). Furthermore, Pacheco-Alvarez et al. reported that phosphorylation of NCC at Thr 53 and 58, and at Ser 71 was important for NCC function in *Xenopus* oocytes (Pacheco-Alvarez et al., 2006), and we showed that phosphorylated NCC is concentrated on the apical membranes of distal convoluted tubules in the $WNK4^{D561A/+}$ knock-in mice, which suggests that phosphorylation may also be important for intracellular localization of NCC (Yang, S. S. et al., 2007). Based on the above evidence, we postulated that WNK, OSR1/SPAK and NCC constitute a signal cascade in the in vivo kidney, which is important for NaCl homeostasis and blood pressure regulation. Recently, we mated $WNK4^{D561A/+}$ knock-in mice with SPAK and OSR1 kinase-dead knock-in mice, in which the T-loop Thr residues in SPAK (Thr 243) and OSR1 (Thr 185) were mutated to Ala to prevent activation by WNK kinases (Rafiqi et al., 2010). In these triple knock-in mice, PHAII phenotypes and increased phosphorylation of NCC were completely corrected (Chiga et al., 2011). Based on the definitive genetic data, we clearly established the presence of the WNK-OSR1/SPAK-NCC kinase cascade in the in vivo kidney.

Although the signal cascade was established, it remains unclear which WNK kinase is responsible in the kidney. It is also uncertain whether a single dominant WNK kinase is present in each different type of cell, or whether multiple WNKs are present in the same cells and function as a WNK kinase complex, as postulated by Yang, C. L. et al. (Yang, C. L. et al., 2007). In fact, in addition to WNK1 and WNK4, whose mutations cause PHAII, WNK3 mRNA expression was reported to be present in

the kidney (Holden et al., 2004). Therefore, although WNK3 mutation has not been observed in PHAII, WNK3 could be an important component of WNK kinase-mediated signal cascade in kidney. Previous in vitro data found that WNK3 regulates SLC12A cotransporters. WNK3 was shown to be an activator of Na-K-Cl cotransporter (NKCC1 and 2) and NCC (Kahle et al., 2005; Rinehart et al., 2005; Yang, C. L. et al., 2007; San-Cristobal et al., 2008; Ponce-Coria et al., 2008; Glover et al., 2009; Cruz-Rangel et al., 2011), and a repressor of K-Cl cotransporters (KCC 1-4) (Kahle et al., 2005; de Los Heros et al., 2006), when co-expressed in *Xenopus laevis* oocytes. Similar to WNK1 and WNK4, WNK3 was found to phosphorylate SPAK in *Xenopus laevis* oocytes (Ponce-Coria et al., 2008).

Previously, WNK4 hypomorphic mice and WNK1 heterozygous mice reportedly showed low blood pressure (Ohta et al., 2009; Zambrowicz et al., 2003). Therefore, we aimed to determine the contribution of WNK3 to WNK-mediated kidney functions by generating WNK3 knockout mice. The data obtained suggest that WNK3 may not play a major role in the WNK kinase cascade in the kidney.

Results

Generation of WNK3 knockout mice

In order to generate WNK3 knockout mice, we planned to delete exon 2 (Fig. 1A), as exon 2 contains the catalytic domain of mouse WNK3 (Holden et al., 2004; Verissimo et al., 2006). We crossed chimeric mice from recombinant ES clones with C57BL/6 mice to produce WNK3 (flox/+) mice. The generation of WNK3 (flox/+) mice was verified by PCR (Fig. 1B). Next, to delete exon 2 from the *Wnk3* gene, we crossed WNK3 (flox/+) female mice with Cre recombinase transgenic male mice. The Cre-mediated excision of exon 2 and Neo cassette was verified by PCR, as shown in Fig. 1C. The absence of WNK3 protein was confirmed by immunoblotting in brain and testis (Fig. 1D). However, due to the low level of WNK3 protein expression in the kidney, WNK3 was not detected by immunoblotting, even in wild-type mouse kidney. To verify that WNK3 is also disrupted in the kidney, we performed RT-PCR of WNK3 and confirmed the absence of WNK3 mRNA in the kidneys of WNK3 knockout mice (Fig. 1E).

Segmental expression of WNK3 along mouse nephron

First, we aimed to determine where WNK3 is expressed along the mouse nephron, as we had to identify the transporters present in the segment where WNK3 is expressed. It was previously reported that, on immunofluorescence, WNK3 is present in all nephron segments (Rinehart et al., 2005). However, because the same antibody did not work both in immunofluorescence and immunoblotting in our hand, we performed laser capture microdissection (LCM) and RT-PCR in order to confirm segmental expression of WNK3 along nephron. As shown in Fig. 2, we confirmed that WNK3 is expressed in proximal tubules, thick ascending limb of Henle's loop (TAL), distal convoluted tubules (DCT) and collecting ducts, where Na/H exchanger 3 (NHE3), NKCC2, NCC and epithelial Na channel (ENaC) are expressed, respectively.

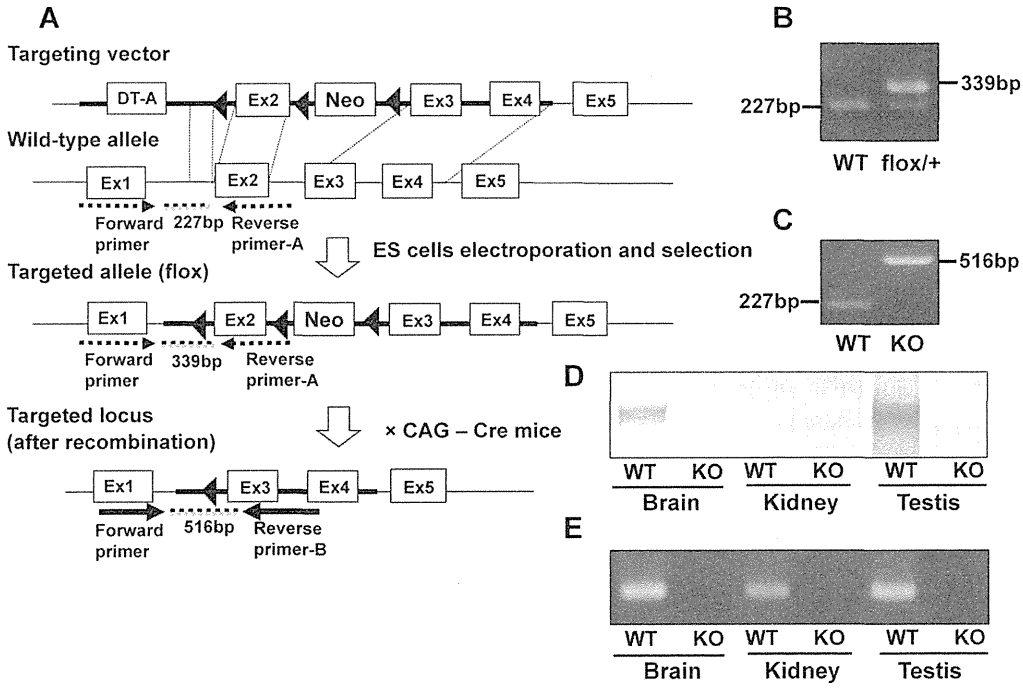

Fig. 1. Generation of WNK3 knockout mice. (A) Targeting strategy for *Wnk3* gene interruption. The diagram shows the targeting construct, the wild-type WNK3 locus, and the targeted locus before and after Cre recombination. Three loxPs were inserted to flank exon 2 and the LacZ-Neo-selective marker. Exon 2 was deleted by mating the flox mice with CAG promoter Cre recombinase mice. **(B)** Verification of homologous recombination by PCR of genomic DNA derived from tails of mice. The primer set is indicated by dotted arrows in A. The 227-bp band and 339-bp band represent the wild-type allele and flox allele, respectively. **(C)** Genotyping PCR after Cre recombination, using a primer set indicated by solid arrows in A. A 516-bp PCR product was specific to the mutant allele. **(D)** Immunoblot of brain, kidney and testis homogenates probed with anti-WNK3 antibody. Absence of WNK3 protein in WNK3 knockout mouse was confirmed by immunoblotting in brain and testis. WNK3 was not detected by immunoblotting, even in wild-type mouse kidney, due to the low level of WNK3 protein expression in the kidney. **(E)** RT-PCR of brain, kidney and testis of wild-type and WNK3 knockout mice.

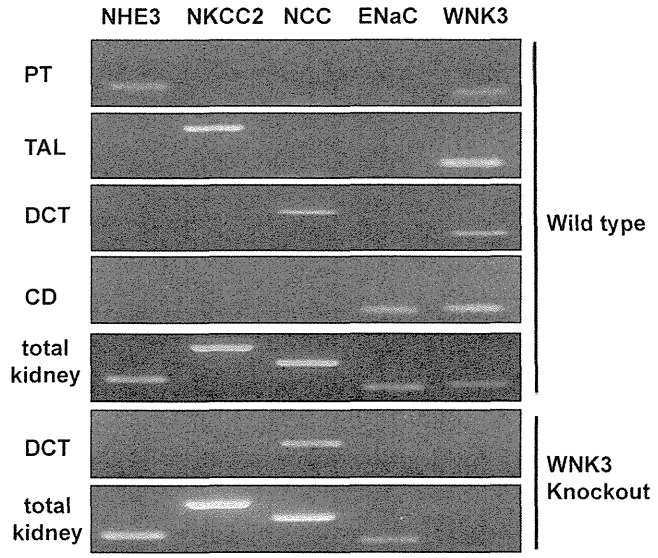

Fig. 2. Segmental expression of WNK3 along mouse nephron. Primers for NHE3, NKCC2, NCC and ENaC were used as markers for each segment. WNK3 was positive in proximal tubules, thick ascending limb of Henle's loop, distal tubules and collecting ducts of wild type mouse. As a negative control, distal tubules and total kidney homogenate from WNK3 knockout mouse were used. PT, proximal tubule; TAL, thick ascending limb of Henle's loop; DCT, distal convoluted tubule; CD, collecting duct.

Blood and urine analysis

We observed no obvious differences between the WNK3 knockout mice and wild-type littermates in survival, gross physical appearance and organ morphology. There were no significant differences in the plasma K^+ and HCO_3^- levels (Table 1). Urine volume and urinary excretion of Na^+ and K^+ under normal conditions were not significantly affected in WNK3 knockout mice. To more thoroughly characterize the phenotypes, we fed WNK3 knockout and wild-type mice low-salt (0.01% NaCl) and high-salt (4% NaCl) diets, and monitored urinary Na^+ and K^+ excretion, particularly focusing on the transition periods while changing diets. However, as shown in Fig. 3A–C, sodium excretion in the WNK3 knockout mice did not change during the experimental period.

Blood pressure

We used a tail-cuff system to measure blood pressure. As shown in Fig. 4A, blood pressure in WNK3 knockout mice did not show any significant differences when compared with wild-type mice under normal diet (109.7±1.6 vs. 111.2±1.6 mmHg, knockout: n=11, wild-type: n=14). However, when mice were fed with low-salt diet, blood pressure in WNK3 knockout mice was lower compared with wild-type mice (105.8±1.1 vs. 110.7±0.7 mmHg, knockout: n=11, wild-type: n=9, P<0.01) (Fig. 4B).

Table 1. Biochemical analysis of blood from wild-type and WNK3 knockout mice

	Wild type (n=9)	WNK3 knockout (n=10)	P Value
Na^+ (mmol/l)	145.8±1.7	144.9±2.0	0.34
K^+ (mmol/l)	4.7±0.4	4.9±0.3	0.17
Cl^- (mmol/l)	113.1±1.1	111.9±1.4	0.07
HCO_3^- (mmol/l)	23.6±1.4	23.8±1.1	0.78
pH (venous)	7.36±0.02	7.35±0.03	0.41

Values in mean ± SD.

Expression and phosphorylation of NCC and NKCC2 were not affected in WNK3 knockout mouse kidney

WNK3 reportedly activates NCC and NKCC2 function when co-expressed in *Xenopus* oocytes. Therefore, we investigated whether expression and phosphorylation of NCC and NKCC2 were decreased in the kidneys of WNK3 knockout mice. However, as shown in Fig. 5A–B, we could not see any significant difference in the protein abundance or the magnitude of phosphorylation of NKCC2 and NCC between WNK3 knockout and wild-type mice under a normal diet. Next, to investigate whether phosphorylation of OSR1 and SPAK was lower due to an absence of WNK3, we examined phosphorylation of OSR1 at 325S and SPAK at 380S, phosphorylation sites for WNK kinases, using phospho-specific antibodies. As shown in Fig. 5C–D, phosphorylation of OSR1 and SPAK at their WNK phosphorylation sites was not lower in kidneys from WNK3 knockout mice.

Furthermore, we examined the phosphorylation status of NCC and NKCC2 in WNK3 knockout mice under low-salt diet, since blood pressure in WNK3 knockout mice was lower, when mice were fed with low-salt diet. However, even under low-salt diet, WNK3 knockout mice did not show decreased phosphorylation of either NCC or NKCC2, when compared with wild-type mice (Fig. 6A–B). These results indicated that WNK3 does not play a major role in regulation of NCC and NKCC2 in vivo mouse kidney, in contrast to several over-expression studies in *Xenopus* oocytes. Phosphorylation of OSR1 and SPAK at their WNK phosphorylation sites was not lower in kidneys from WNK3 knockout mice, even under low-salt diet (Fig. 6C–D).

Expression of NHE3 and γ-ENaC in the kidneys of WNK3 knockout mice was not significantly different from that in wild-type mice (supplementary material Fig. S1).

Expression levels of WNK4 were elevated in kidneys of WNK3 knockout mice

The WNK kinase family phosphorylates and activates OSR1 and SPAK, and activated OSR1 and SPAK kinases phosphorylate NCC. We hypothesized that other WNKs could compensate for the absence of WNK3 in the kidney. To examine this hypothesis, we examine the expression levels of WNK1 and WNK4 in the kidneys of WNK3 knockout mice. As shown in Fig. 7A–B, we found that WNK4 expression was slightly but significantly elevated in kidneys from WNK3 knockout mice, as compared to those from wild-type mice. We also examined WNK1 and WNK4 expression in WNK3 knockout mice fed low-salt diet, as compensation would become clearer when the WNK-OSR1/SPAK-NCC phosphorylation cascade is activated (Chiga et al., 2008). As expected, under low-salt diet, both WNK1 and WNK4 expression increased significantly in kidneys from WNK3 knockout mice, as compared to wild-type mice (Fig. 7C–D). These results indicate that increased expression of WNK1 and WNK4 compensate for the absence of WNK3 in kidneys from WNK3 knockout mice.

Discussion

One of the major issues in hypertension research is regulation of renal sodium transporters that control sodium reabsorption in the